

The GN-Model of Fiber Non-Linear Propagation and its Applications

Original

The GN-Model of Fiber Non-Linear Propagation and its Applications / Poggiolini, Pierluigi; Bosco, Gabriella; Carena, Andrea; Curri, Vittorio; Jiang, Yanchao; F., Forghieri. - In: JOURNAL OF LIGHTWAVE TECHNOLOGY. - ISSN 0733-8724. - STAMPA. - 32:4(2014), pp. 694-721. [10.1109/JLT.2013.2295208]

Availability:

This version is available at: 11583/2542088 since:

Publisher:

IEEE / Institute of Electrical and Electronics Engineers

Published

DOI:10.1109/JLT.2013.2295208

Terms of use:

openAccess

This article is made available under terms and conditions as specified in the corresponding bibliographic description in the repository

Publisher copyright

(Article begins on next page)

The GN-Model of Fiber Non-Linear Propagation and its Applications

P. Poggiolini, *Member, IEEE*, G. Bosco, *Member, IEEE*, A. Carena, *Member, IEEE*, V. Curri, *Member, IEEE*, F. Forghieri, *Member, IEEE*

Abstract—Several approximate non-linear fiber propagation models have been proposed over the years. Recent re-consideration and extension of earlier modeling efforts has led to the formalization of the so-called Gaussian-Noise (GN) model.

The evidence collected so far hints at the GN-model as being a relatively simple and, at the same time, sufficiently reliable tool for performance prediction of uncompensated coherent systems, characterized by a favorable accuracy vs. complexity trade-off.

This paper tries to pull together the recent results regarding the GN-model definition, understanding, relations vs. other models, validation, limitations, closed form solutions, approximations and, in general, its applications and implications in link analysis and optimization, also within a network environment.

Index Terms—coherent systems, uncompensated transmission, non-linear effects, GN-model, PM-QAM

I. INTRODUCTION

THE advent of coherent-detection systems supported by digital-signal-processing (DSP) has made it possible to carry out *electronic* fiber chromatic-dispersion (CD) compensation. This in turn has permitted to avoid *optical* dispersion compensation, or dispersion management (DM), thus allowing the exploitation of the so-called ‘uncompensated’ transmission (UT) technique.

The UT scenario has proved quite advantageous in a number of ways. Repeaters, not needing to support the insertion of dispersion-compensating units, have become simpler and hence cheaper and better performing. More important, it was recognized early on that links based on UT are less impacted by non-linearity than DM links. As a result, UT has become the solution of choice for green-field installations, as well as for overhauling and upgrading existing links where DM removal is practically and economically feasible.

Finally, as a subtler by-product of UT adoption, it has been recognized that certain perturbative models of fiber non-linear propagation, which did not work satisfactorily with DM, can instead provide rather accurate system performance prediction with UT. In particular, recent re-consideration and extension of earlier modeling efforts has led to the formalization of the so-called Gaussian-Noise (GN) model.

The GN-model is just one of several perturbative models that have been proposed over the years. However, the GN-model has proved itself a relatively simple and, at the same

time, sufficiently reliable tool for performance prediction over a wide range of system scenarios, effective for both system analysis and design.

This paper tries to pull together the recent results regarding the GN-model definition, understanding, relations vs. other models, validation, limitations, closed-form solutions, approximations and, in general, its applications and implications in link analysis and optimization, also within a network environment.

Overall, the fiber non-linearity modeling effort is far from over and new models or variations on existing ones are being published at an increasing rate. This is a positive process and certainly the next few years will see continuous improvement and refinement, most likely leading to ever more effective models.

The paper is structured as follows.

In Sect. II an overview of certain classes of perturbative models and of the most common assumptions made to derive them is proposed. In Sect. III, the GN-model reference formulas are introduced and a physical interpretation of the model is proposed. The incoherent GN-model (IGN-model), a simplified variant to the GN-model, is presented and discussed. Sect. IV is devoted to the use of the GN-model to assess system performance. A discussion of the impact on system performance evaluation of possible inaccuracy in non-linearity estimation is proposed. Sect. V focuses on a broad-range simulative validation of the GN-model. The errors and limitations due to the approximations used by the model are studied in detail. Sect. VI collects various analytical closed-form results obtained from the GN-model. Sect. VII deals with the derivation from the GN-model of practical simplified system design rules, which are then validated vs. experimental results and discussed. In Sect. VIII, the GN-model is used to obtain non-linear optical channel throughput estimates. The throughput of practical links is also evaluated and discussed. The potential effectiveness of DSP-enabled non-linear mitigation techniques is investigated in Sect. IX, based on the GN-model. Sect. X is devoted to the use of the GN-model in the context of the control and optimization of transparent flexible optical networks. Comments and conclusion follow.

A complete list of the acronyms used in this paper is provided in Appendix A.

II. AN OVERVIEW OF SOME UT PERTURBATIVE MODELS

Many approximate fiber non-linear propagation models have been proposed and studied over the years [3]-[47], addressing very different link and system scenarios as technology evolved.

P. Poggiolini, G. Bosco, A. Carena and V. Curri are with Politecnico di Torino, Dipartimento di Elettronica, C.so Duca Degli Abruzzi 24, 10129 Torino, Italy. E-mail: pierluigi.poggiolini@polito.it, website: <http://www.optcom.polito.it>.

F. Forghieri is with Cisco Photonics Italy s.r.l., via Philips 12, 20900 Monza, Italy. E-mail: fforghie@cisco.com.

Here we collect those models that are specific to UT and that appear to be more directly related to the GN-model. We also discuss a few other models that are less similar to the GN-model but have certain features that are of relevance in the context of the discussion of the GN-model. We follow a similar classification as in [34], [36], with some changes and the addition of more recent developments.

We first introduce three of the most common assumptions made in deriving approximate non-linear propagation models for UT.

A. Most common modeling assumptions

The majority of non-linear propagation models make the assumption that non-linearity is relatively small, i.e., that it is a *perturbation* as compared to the useful signal. Thanks to this assumption, model derivation can exploit *perturbation* techniques, which allow to find approximate analytical solutions to the non-linear Schroedinger equation (NLSE) or the Manakov (ME) equation [1], [2]. Clearly, the perturbation assumption breaks down at highly non-linear regimes. However, both simulations and experiments have shown it to be sufficiently well verified within the range of optimal system launch powers. Its validity will be discussed in Sect. V. All models mentioned in the following are perturbation analysis models, although the specific perturbation technique may differ.

A second assumption is that the transmitted signal statistically behaves as stationary Gaussian noise. We call this the ‘signal-Gaussianity’ assumption. This assumption is certainly not verified at the Tx output. However, it can be argued that, as the signal propagates along a UT link and gets thoroughly dispersed, it tends to take on an approximately Gaussian-like distribution.

Another common assumption is that the signal disturbance generated by non-linearity, which we call throughout this paper *non-linear interference* (NLI), manifests itself as *additive Gaussian noise* (AGN).

All these assumptions are just tentative *approximations* that have been used to derive models that typically do not aim at being exact solutions of the non-linear propagation problem. Like the GN-model, they generally aim at being practical tools, sufficiently accurate to be used for system analysis and design. Given the approximations involved, their effectiveness must be established a posteriori through proper validation. This is discussed in Sect. V, where the GN-model predictive performance is extensively tested over a broad range of system scenarios. The model inaccuracy due to the above assumptions and, in particular, to the signal Gaussianity assumption, is thoroughly analyzed.

B. Model classes

We first introduce those models that lead to results that are close or coincident with those of the GN-model. They make use of *all three assumptions* mentioned in Sect. II-A

The earliest of these models dates back to 1993 [28]. It was based on directly postulating that all non-linearity was produced by FWM acting among the overall WDM signal spectral

components, assumed ‘incoherent’. Remarkably, though limited to single-polarization and to a rectangular overall WDM spectrum, the results of this early effort essentially agree with those obtained through the GN-model under such limitations. In 2003, [29] showed that, based on a perturbation approach outlined in [10], similar results to those found in [28] could be re-derived.

A 1997 paper [39] found an approximate solution to the NLSE in terms of a truncated Volterra series (VS) in frequency domain. These results were later used (in 2002) to derive a PSD of NLI [40] and to discuss fiber capacity in [41], in a single-polarization scenario. The found model equations are very similar to the GN-model for single-polarization.

More recently, another approach was proposed, based on ideally slicing up the signal spectrum into discrete spectral components, whose non-linear beating during propagation is then analytically assessed. We call it the Spectral Slicing (SpS) approach. Spectral slicing is naturally found in OFDM systems, so SpS was first used to model non-linearity limited to these systems (2008-2011) [30]–[32]. These papers obtained what could be viewed as a specialized version of the GN-model for OFDM.

The SpS approach was also taken up aiming at general WDM systems (including OFDM as a special case). In this approach, spectral slicing is introduced early in the derivation but then it is removed through a suitable transition to continuous spectra. This effort (2011 to now [33]–[36]) led to the first appearance of the GN-model in its current form.

Two further papers, devoted specifically to detailed re-derivations of the GN-model, were also recently published (2011-2013) [37]–[38]. Both independently confirm the GN-model main equations and provide some generalizations. Specifically, [37] is based on an modified version of the first-order regular-perturbation method (RP1), which had been shown in [12] to be equivalent to the VS method. Paper [38] uses a variation on the SpS approach.

An interesting question is why the earlier instances of these models did not enjoy widespread attention when originally published many years ago. The answer appears to be that they did not work well for the DM systems of the time. Specifically, it appears that the signal-Gaussianity assumption does not hold up well, or not at all, in DM systems where, contrary to UT, dispersion is not allowed to accumulate.

A separate class of proposed models employs a time-domain (TD) perturbation approach, which was introduced in 2000 [42], [43]. In 2012, this approach was substantially re-visited and extended [44], [45]. The interesting feature of the TD models is that they do not need to rely on the signal-Gaussianity assumption, ideally making it possible for them to overcome the GN-model limitations induced by the signal-Gaussianity assumption (see Sect. V-C).

However, without signal-Gaussianity, rather complex equations are found. In order to achieve simpler results, further assumptions and approximations are typically necessary. For instance, in [43] an approximate closed-form relation for the total NLI noise power for a single-channel is found, but a ‘phase-incoherence’ assumption (roughly corresponding to the signal-Gaussianity assumption) is needed to derive it.

Incidentally, the final formula bears substantial similarity to Eq. (37) of this paper, derived through the GN-model, showing once more that result convergence is found among different models when the same assumptions are made.

Over the last few months, various other models have been proposed. These include a discrete-time single-channel model based on deriving analytical results from the split-step algorithm [46]. Another proposal makes use of a more conventional perturbative approach: however, instead of seeking a result in terms of an additive NLI disturbance, it looks at phase disturbance, akin to self- and cross-phase modulation (SPM and XPM) [47].

As a whole, research on the topic of non-linearity modeling is quite active and new models and results may be expected in the near future¹.

III. THE GN MODEL REFERENCE FORMULA

The GNRF supplies $G_{\text{NLI}}(f)$, that is, the PSD of NLI at the end of the link. In this section, the GNRF is introduced, first in a general form, capable of dealing with a very wide variety of systems, and then in a simpler form, valid under restrictive system constraints, which however makes it easy to extract an intuitive physical explanation of the phenomena it describes. Finally, a simplified variant to the GN-model will be introduced and its features discussed.

A. The general form of the GNRF

The symbols most frequently used in the following are listed here for convenience:

- z : the longitudinal spatial coordinate, along the link [km]
- α : fiber *field* loss coefficient [km^{-1}], such that the signal *power* is attenuated as $\exp(-2\alpha z)$
- $g(z)$: fiber *field* gain coefficient [km^{-1}], possibly z -dependent, such that the signal *power* is amplified over a stretch of z km as $\int_0^z \exp(2g(z'))dz'$
- Γ : lumped power gain, such as due to an EDFA
- β_2 : dispersion coefficient in [$\text{ps}^2 \cdot \text{km}^{-1}$]
- β_3 : dispersion slope in [$\text{ps}^3 \cdot \text{km}^{-1}$]
- β_{DCU} : lumped accumulated dispersion in [ps^2]
- γ : fiber non-linearity coefficient [$\text{W}^{-1} \cdot \text{km}^{-1}$]
- L_s : span length [km]
- L_{eff} : span effective length [km]
- N_s : total number of spans in a link
- $G_{\text{WDM}}(f)$: PSD of the overall WDM transmitted signal

Note that in this paper all PSDs are assumed to be *unilateral*.

As mentioned in Sect. II, the derivation of the GNRF was extensively dealt with in [34]-[38] and will not be addressed here. This version of the GNRF makes the following assumptions:

- the transmitted signals are dual-polarization
- a ‘span’ consists of a single fiber type.

¹After submission and first revision of this paper, various new theoretical contributions have appeared on non-linearity modeling. They are too recent to take their results into account here. However, we include them in the bibliography for future reference, as they appear to contain significant new results [48]-[51].

Note that the latter restriction is only apparent: if an actual link has a span that harbors more than one fiber type, such span can be formally broken up into multiple spans, one for each fiber type.

The GNRF can then be written as follows [35]:

$$G_{\text{NLI}}(f) = \frac{16}{27} \int_{-\infty}^{\infty} \int_{-\infty}^{\infty} G_{\text{WDM}}(f_1) G_{\text{WDM}}(f_2) G_{\text{WDM}}(f_1 + f_2 - f) \left[\sum_{n=1}^{N_s} \gamma_n \left[\prod_{k=1}^{n-1} \exp \left(\int_0^{L_{s,k}} 3g_k(\zeta) d\zeta \right) \exp(-3\alpha_k L_{s,k}) \Gamma_k^{3/2} \right] \left[\prod_{k=n}^{N_s} \exp \left(\int_0^{L_{s,k}} g_k(\zeta) d\zeta \right) \exp(-\alpha_k L_{s,k}) \Gamma_k^{1/2} \right] \exp(j4\pi^2 (f_1 - f)(f_2 - f) \cdot \sum_{k=1}^{n-1} [\beta_{2,k} L_{s,k} + \pi (f_1 + f_2) \beta_{3,k} L_{s,k} + \beta_{\text{DCU},k}]) \int_0^{L_{s,n}} [\exp \left(\int_0^z 2g_n(\zeta) d\zeta - 2\alpha_n z \right) \exp(j4\pi^2 (f_1 - f)(f_2 - f) \cdot [\beta_{2,n} + \pi\beta_{3,n}(f_1 + f_2)] z)] dz \right]^2 df_1 df_2 \quad (1)$$

where Γ_k is lumped power-gain placed immediately following the k -th span and g_k is the possible distributed field-gain (such as due to Raman amplification) occurring along the k -th span. In general, integer subscripts such as k , n , indicate to which span a certain quantity is referred.

This equation can take into account lumped dispersive elements placed at the end of each span, through the parameter β_{DCU} . However, the presence of such elements may cause the signal-Gaussianity assumption to degrade. In this paper we will always assume $\beta_{\text{DCU}}=0$ (pure UT) and leave the investigation of any inaccuracy issues in the presence of lumped dispersive elements for future investigation.

B. Physical interpretation of the GN-model

Eq. (1) is quite general but rather involved. To discuss the physical interpretation of the GN-model, we further assume that:

- the link is made up of identical spans (the *homogenous link* assumption)
- the loss of each span, including the last one, is exactly compensated for by optical amplification (the *transparent link* assumption).

As a result, the GNRF can be written as:

$$G_{\text{NLI}}(f) = \frac{16}{27} \gamma^2 L_{\text{eff}}^2 \int_{-\infty}^{\infty} \int_{-\infty}^{\infty} G_{\text{WDM}}(f_1) G_{\text{WDM}}(f_2) G_{\text{WDM}}(f_1 + f_2 - f) \cdot \rho(f_1, f_2, f) \cdot \chi(f_1, f_2, f) df_2 df_1 \quad (2)$$

Then, the formula can be given the following physical interpretation: the NLI PSD generated at a frequency f , that is $G_{\text{NLI}}(f)$, is the integrated result of all the ‘infinitesimal’ non-degenerate FWM products occurring among any three spectral components of the transmitted signal, located at f_1 , f_2 and $f_3 = (f_1 + f_2 - f)$.

In fact, the integrand factor:

$$G_{\text{WDM}}(f_1) G_{\text{WDM}}(f_2) G_{\text{WDM}}(f_1 + f_2 - f) \quad (3)$$

is directly related to the FWM process as it is the product of three signal frequency components that act as a ‘pumps’ for the FWM process itself. Fig. 1 shows four instances of such triads of pumps, all creating NLI at frequency f . The integrand factor $\rho(f_1, f_2, f)$ can be shown to be the non-degenerate FWM efficiency of their beating, assumed to be normalized so that its maximum is 1. Its general definition, as it applies to Eq. (2), is:

$$\rho(f_1, f_2, f) = \left| \int_0^{L_s} e^{\int_0^z 2g(\zeta) d\zeta} e^{-2\alpha z} e^{j4\pi^2(f_1-f)(f_2-f)[\beta_2+\pi\beta_3(f_1+f_2)]z} dz \right|^2 / L_{\text{eff}}^2 \quad (4)$$

with:

$$L_{\text{eff}}^2 = \left| \int_0^{L_s} e^{\int_0^z 2g(\zeta) d\zeta} e^{-2\alpha z} dz \right|^2 \quad (5)$$

The specific form taken on by ρ depends on the type of amplification used. For example, assuming lumped amplification (EDFA-like), ρ takes on the following closed-form [53]:

$$\rho(f_1, f_2, f) = \frac{\left| 1 - e^{-2\alpha L_s} e^{j4\pi^2(f_1-f)(f_2-f)[\beta_2+\pi\beta_3(f_1+f_2)]L_s} \right|^2}{\left| 2\alpha - j4\pi^2(f_1-f)(f_2-f)[\beta_2+\pi\beta_3(f_1+f_2)] \right|^2} L_{\text{eff}}^{-2} \quad (6)$$

with:

$$L_{\text{eff}} = (1 - e^{-2\alpha L_s}) / 2\alpha \quad (7)$$

In the case of distributed amplification Eqs. (4)-(5) generate different expressions for ρ (see Sect. VI) but this does not affect its physical meaning.

Finally, the factor χ is:

$$\chi(f_1, f_2, f) = \frac{\sin^2(2N_s\pi^2(f_1-f)(f_2-f)[\beta_2+\pi\beta_3(f_1+f_2)]L_s)}{\sin^2(2\pi^2(f_1-f)(f_2-f)[\beta_2+\pi\beta_3(f_1+f_2)]L_s)} \quad (8)$$

Note that if the link consists of a single span, then $\chi = 1$. Therefore this factor clearly has the role of accounting for NLI accumulation in multi-span links. In fact, it takes into account the coherent interference at the Rx location of the NLI produced in each span. It is sometimes called ‘phased-array factor’ since it is formally identical to the radiation pattern of a phased-array antenna. A similar interference pattern, with the same analytical form, emerged in the context of conventional FWM calculations [53], [54] and was discussed in detail in [30] in the context of OFDM systems. The factor χ is quite important and will be discussed in various other sections of this paper.

We would like to remark that the GNRF, in either its more general (1) or its simpler form (2), is not derived using the *a priori* assumption that the dominant non-linear phenomenon is FWM. All recent detailed derivations [35], [37], [38] actually start from the Manakov equation and rigorously apply only the three assumptions discussed in Sect. II-A, which do not specifically pre-suppose FWM. It is at the end of the derivation, i.e., *a posteriori*, that the integrand function within the GNRF can be recognized as representing an infinitesimal non-degenerate FWM contribution, as described above.

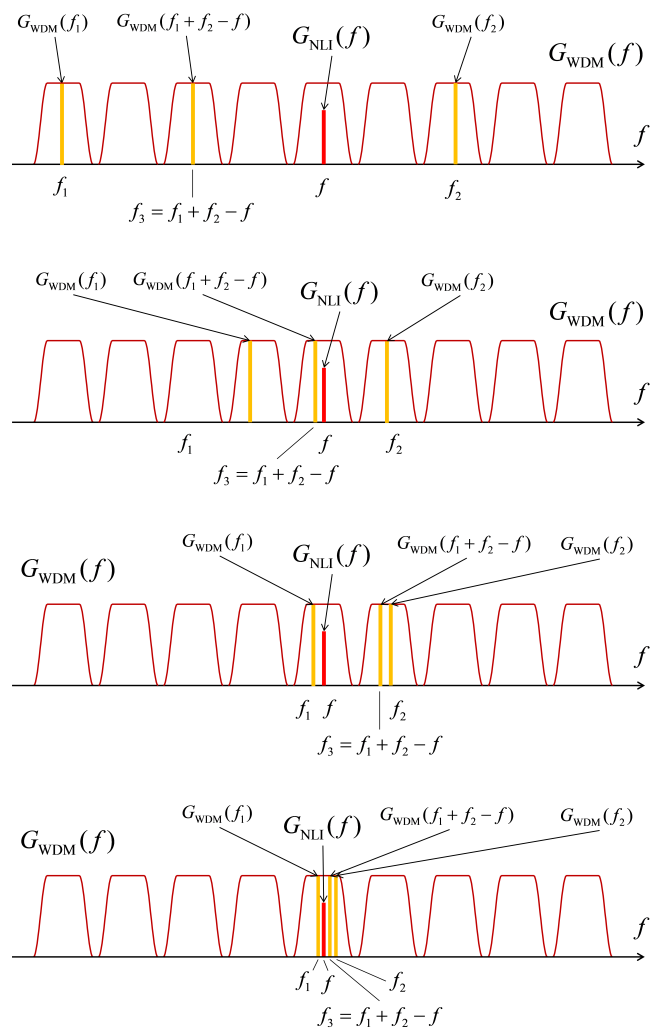


Fig. 1. Four instances of signal frequency component triads (yellow bars) contributing to creating FWM-induced NLI at frequency f (red bar). The two top triads generate MCI, the third from top XCI and the bottom one SCI.

This physical interpretation, which ascribes all NLI to FWM, brings about the question of whether the non-linear phenomena taxonomy formerly used for DM systems, such as SPM, XPM, and XPolM, can still be related to UT systems as represented through the GN-model. This topic was discussed in some depth in [36]. There, it was argued that NLI has features quite different from those implied by the old taxonomy. As an example, although in the GN-model it is still possible to single out the NLI produced by one channel onto itself, it would be somewhat misleading to call it SPM because NLI behaves approximately as additive Gaussian noise, far from the highly structured and deterministic pulse-distortion effect caused by SPM.

In [36], a possible alternative taxonomy was proposed, consisting of three categories: self-channel interference (SCI), cross-channel interference (XCI) and multi-channel interference (MCI). Specifically:

- SCI is the NLI perturbing a given channel, produced by that channel onto itself
- XCI is the NLI perturbing a given channel, produced by the non-linear interaction of that channel with *one* other

channel

- MCI is the NLI perturbing a given channel, produced by the non-linear interaction of that channel with *two other channels* or by *three channels other than the affected one*.

Note that all these noise categories approximately manifest themselves as additive Gaussian noise: what makes them different is just their spectral origin, as shown in Fig. 1. There is however, a practical distinction: typically MCI is negligible. This circumstance can be used for instance to help in the derivation of approximate closed-form GNRF solution (Sect. VI). For more details on this taxonomy, see [36], Sect. VI.

C. The IGN-model

In the previous section we have shown that the GNRF accounts for the coherent interference that occurs at the Rx among the NLI generated in each single span. As discussed in Sect. III-B, in the transparent and homogenous link scenario such interference shows up as the GNRF integrand factor χ .

We introduce here an alternative model which coincides with the GN-model over each single span but makes the further approximation of completely neglecting coherent interference among NLI generated in different spans. This model is called the *incoherent* GN-model, or IGN-model. According to it, the total NLI PSD at the end of the link is simply:

$$G_{\text{NLI}}^{\text{inc}}(f) = \sum_{n=1}^{N_s} G_{\text{NLI}}^n(f) \quad (9)$$

where $G_{\text{NLI}}^n(f)$ is the NLI PSD generated in the n -th span alone, then propagated through the link all the way to the Rx. It can be written as:

$$G_{\text{NLI}}^n(f) = \frac{16}{27} \gamma_n^2 L_{\text{eff},n}^2 \prod_{k=1}^{n-1} e^{6 \int_0^{L_{s,k}} g_k(\zeta) d\zeta} e^{-6\alpha_k L_{s,k}} \Gamma_k^3 \prod_{k=n}^{N_s} e^{2 \int_0^{L_{s,k}} g_k(\zeta) d\zeta} e^{-2\alpha_k L_{s,k}} \Gamma_k \int_{-\infty}^{\infty} \int_{-\infty}^{\infty} G_{\text{WDM}}(f_1) G_{\text{WDM}}(f_2) G_{\text{WDM}}(f_1 + f_2 - f) \rho_{n,s}(f_1, f_2, f) df_1 df_2 \quad (10)$$

where the integer subscripts n, k , indicate the span to which a certain quantity is referred.

Eqs. (9)-(10) constitute the generalized incoherent-GNRF, or IGNRF. Assuming a transparent and homogeneous link, the IGNRF greatly simplifies to:

$$G_{\text{NLI}}^{\text{inc}}(f) = \frac{16}{27} \gamma^2 L_{\text{eff}}^2 N_s \int_{-\infty}^{\infty} \int_{-\infty}^{\infty} G_{\text{WDM}}(f_1) G_{\text{WDM}}(f_2) G_{\text{WDM}}(f_1 + f_2 - f) \rho(f_1, f_2, f) df_1 df_2 \quad (11)$$

D. Comparison of GN vs. IGN model

The approximation leading to the IGN model appears at first quite drastic and arbitrary. In reality, it can be justified based on various arguments. Here, for simplicity, we address this topic in the context of transparent and homogenous links. We

also assume $\beta_3=0$. The results can be extended to the more general cases.

We start out by remarking that the phased-array factor χ of Eq. (8) can also be written in finite sum form as:

$$\chi(f_1, f_2, f) = N_s + 2 \sum_{n=1}^{N_s-1} (N_s - n) \cdot \cos(4n \pi^2 \beta_2 L_s (f_1 - f)(f_2 - f)) \quad (12)$$

When this alternative expression is inserted into the GNRF of Eq. (2), the latter can formally be split into two contributions:

$$G_{\text{NLI}}(f) = G_{\text{NLI}}^{\text{inc}}(f) + G_{\text{NLI}}^{\text{cc}}(f) \quad (13)$$

where $G_{\text{NLI}}^{\text{inc}}$ is the IGNRF Eq. (11). This clearly shows that the IGN-model is based on retaining only the first contribution in Eq. (13). This approximation makes sense only if the second contribution, that we call *coherence correction*, can be considered small. Its expression is:

$$G_{\text{NLI}}^{\text{cc}}(f) = \frac{32}{27} \gamma^2 L_{\text{eff}}^2 \sum_{n=1}^{N_s-1} (N_s - n) \cdot \int_{-\infty}^{\infty} \int_{-\infty}^{\infty} G_{\text{WDM}}(f_1) G_{\text{WDM}}(f_2) G_{\text{WDM}}(f_1 + f_2 - f) \cdot \rho(f_1, f_2, f) \cdot \cos(n \cdot 4\pi^2 \beta_2 L_s (f_1 - f)(f_2 - f)) df_2 df_1 \quad (14)$$

The conjecture that $G_{\text{NLI}}^{\text{cc}}$ may be small vs. $G_{\text{NLI}}^{\text{inc}}$ can be justified based on the fact that the integrand function within $G_{\text{NLI}}^{\text{cc}}$ has the *same, always-positive factors* as $G_{\text{NLI}}^{\text{inc}}$, but in $G_{\text{NLI}}^{\text{cc}}$ they are multiplied times an oscillating cosine factor that tends to cancel out their contributions. This qualitative argument is compelling but of course validation is needed.

An effective way to confirm this conjecture, and hence the validity of the IGN model, is to directly compare the overall IGN and GN-model predictions in terms of NLI noise accumulation vs. number of spans, as follows. The IGN and GN models can be formally re-written as:

$$G_{\text{NLI}}^{\text{inc}}(f) = G_{\text{NLI}}^{1 \text{ span}}(f) \cdot N_s \quad (15)$$

$$G_{\text{NLI}}(f) = G_{\text{NLI}}^{1 \text{ span}}(f) \cdot N_s^{1+\epsilon} \quad (16)$$

where $G_{\text{NLI}}^{1 \text{ span}}$ is the NLI produced in a single span:

$$G_{\text{NLI}}^{1 \text{ span}}(f) = \frac{16}{27} \gamma^2 L_{\text{eff}}^2 \int_{-\infty}^{\infty} \int_{-\infty}^{\infty} G_{\text{WDM}}(f_1) G_{\text{WDM}}(f_2) G_{\text{WDM}}(f_1 + f_2 - f) \rho(f_1, f_2, f) df_1 df_2 \quad (17)$$

Eq. (16), or closely related formulas, have been suggested based on theoretical arguments in several papers, among which [43], [45], [36], [65]. Here, we introduce it without making any approximation with respect to the GNRF Eq. (2), by formally defining ϵ as:

$$\epsilon = \log_e \left(1 + \frac{G_{\text{NLI}}^{\text{cc}}(f)}{G_{\text{NLI}}^{\text{inc}}(f)} \right) \cdot \frac{1}{\log_e(N_s)} \quad (18)$$

In general, ϵ is a function of f and of all system parameters. Remarkably, however, the indication from the above-mentioned theoretical papers, the direct numerical evaluation of Eq. (18), as well as recent experimental results [62], [63] [64], [52], [77], indicate that ϵ is essentially a constant vs. N_s ,

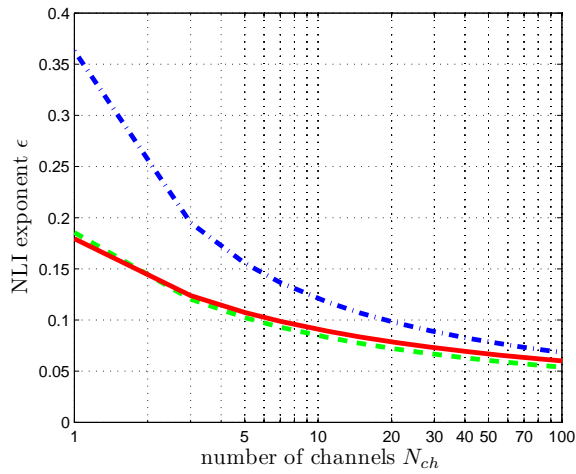


Fig. 2. NLI accumulation exponent ϵ , vs. number of channels N_{ch} . System data: 32 GBaud, 50 GHz channel spacing, raised cosine spectra with roll-off 0.2, span length 100 km. Red solid line: PSCF; green dashed line: SMF; blue dash-dotted line: NZDSF.

in typical links. In particular, it is a positive constant, much smaller than one. For fully-populated (C-band) WDM systems, the typical values of ϵ are between 0.03 and 0.08, depending on system parameters [36]. These small values of ϵ indicate that the difference between the IGN-model of Eq. (15), which predicts purely linear NLI accumulation vs. N_s , and the GN-model of Eq. (16), which predicts slightly super-linear NLI accumulation vs. N_s , is quite small.

A detailed study ([36], Sect. IX) has shown that ϵ depends on the total number of channels in the WDM comb. In Fig. 2, the values of ϵ vs. N_{ch} are shown, for a typical system with 32 GBaud channels and 50 GHz spacing, raised cosine spectra with roll-off 0.2, operated over typical SMF, PSCF and NZDSF (with similar parameters to those of Table I). The plot shows that ϵ gets smaller as the number of channels increases and peaks for single-channel. The physical interpretation of this trend is that the ϵ of NLI due to SCI is rather large, whereas the ϵ of NLI due to XCI and MCI is virtually zero. For single channel, only SCI is present and hence ϵ is large. As the number of channels goes up, the fraction of the overall NLI due to MCI and especially XCI prevails, bringing the overall NLI ϵ towards zero.

In essence, the IGN-model can be expected to practically coincide with the GN-model for systems with a large number of channels, that make use of a substantial part of the C-band. In these scenarios, the IGN-model becomes very attractive because its simpler analytical form makes it much easier to handle and exploit than the GN-model. Caution must instead be used for few-channel systems. For single-channel systems, the IGN model may be rather inaccurate and should not be used. In Sect. V, the predictions of the IGN-model will be carefully compared vs. the GN-model and vs. simulation results, over a wide range of system set-ups.

IV. SYSTEM PERFORMANCE ESTIMATION

So far, we have shown that the GN-model allows to estimate the PSD of NLI at the Rx. Here we address the topic of how

to use this information to assess system performance.

Customarily, the performance of optical coherent systems in *linearity* is estimated by means of the optical signal-to-noise-ratio (OSNR), defined as:

$$\text{OSNR} = \frac{P_{ch}}{P_{ASE}} \quad (19)$$

where P_{ch} is the average power per channel and P_{ASE} is the power of ASE noise which falls within a conventional optical noise bandwidth B_N . To find the BER, the OSNR is inserted into a suitable formula, which depends on the transmission format, the symbol rate R_s and on the chosen value for B_N . For instance, for PM-QPSK, the BER formula is:

$$\text{BER}_{\text{PM-QPSK}} = \frac{1}{2} \text{erfc} \left(\sqrt{\frac{B_N}{2R_s} \text{OSNR}} \right) \quad (20)$$

Similar formulas for the other main QAM formats can be found in [34], App. A.

Note that Eq. (20), as well as textbook formulas addressing other formats, assume that the Rx operates by filtering the incoming signal through a *baseband* transfer function $H_{Rx}(f)$ that is *matched* to the transmitted signal *baseband* pulse. They also assume that inter-symbol interference (ISI) be absent. Otherwise, they are no longer valid, in the sense that there is a penalty with respect to what they predict.

In modern coherent systems, the DSP adaptive equalizer tends to make $H_{Rx}(f)$ converge to a matched shape, so that this condition is typically well satisfied. In this paper, we assume matched $H_{Rx}(f)$ and no ISI.

We then remark that if B_N is set equal to R_s , all OSNR vs. BER laws, such as Eq. (20), become invariant vs. the symbol rate. In this paper we always assume $B_N=R_s$. In order to avoid ambiguity, instead of OSNR, we use the acronym ‘SNR’ to indicate:

$$\text{SNR} = \frac{P_{ch}}{P_{ASE}|_{B_N=R_s}} \quad (21)$$

As a further justification for this definition of signal-to-noise ratio, and for dropping the reference to ‘optical’ in the acronym, we point out that the above SNR, under the mentioned assumptions of a matched $H_{Rx}(f)$ and no ISI, also corresponds exactly to the signal-to-noise ratio that can be directly measured on the Rx electrical signal constellation, at the input of the decision stage. In addition, such SNR also coincides with the communications theory widely used parameter ‘energy-per-symbol vs. noise spectral density’ [55], [56], that is:

$$\text{SNR} = E_s/N_0$$

So far, we have addressed performance in linearity. As discussed in Sect. II-A, NLI noise is assumed to be approximately Gaussian and additive, similar to ASE. Moreover, ASE and NLI are assumed to be uncorrelated. Then, it can be argued that their powers can simply be added at the denominator of the SNR, giving rise to a non-linearity-inclusive SNR:

$$\text{SNR}_{\text{NL}} = \frac{P_{ch}}{P_{ASE} + P_{\text{NLI}}} \quad (22)$$

where P_{NLI} is a suitably-calculated power of NLI noise.

While the PSD of ASE noise $G_{\text{ASE}}(f)$ is certainly flat, or ‘locally white’, over the bandwidth of a single channel, this is not the case, in general, for the PSD of NLI. Therefore, while the correct formula for P_{ASE} in Eq. (22) is simply:

$$P_{\text{ASE}} = G_{\text{ASE}}(f_{\text{ch}}) \cdot R_s \quad (23)$$

where f_{ch} represents the center frequency of the channel under test, the correct formula for P_{NLI} is:

$$P_{\text{NLI}} = \frac{R_s}{B_H} \int_{-\infty}^{\infty} G_{\text{NLI}}(f + f_{\text{ch}}) |H_{\text{Rx}}(f)|^2 df \quad (24)$$

where B_H is:

$$B_H = \int_{-\infty}^{\infty} |H_{\text{Rx}}(f)|^2 df \quad (25)$$

For further details, see [34], Sect. II.A.

The need to use Eqs. (24)-(25) to find P_{NLI} makes BER estimation rather complex. Ideally, it requires the detailed knowledge of both $|H_{\text{Rx}}(f)|^2$ and of $G_{\text{NLI}}(f)$. If, as an approximation, it could be assumed that $G_{\text{NLI}}(f)$ was locally white across the bandwidth spanned by $H_{\text{Rx}}(f)$, then P_{NLI} could be found, similar to ASE noise, simply as:

$$P_{\text{NLI}} = G_{\text{NLI}}(f_{\text{ch}}) \cdot R_s \quad (26)$$

This would require estimating $G_{\text{NLI}}(f)$ at only one frequency and it would allow to completely disregard $H_{\text{Rx}}(f)$. We call this the ‘locally-white noise’ (LWN) approximation.

The possible inaccuracy caused by the LWN approximation will be investigated in Sect. IV-B. Before that, in the next section, we discuss the impact on system performance assessment of any generic inaccuracy incurred in the estimation of P_{NLI} .

A. Impact of inaccuracy in P_{NLI} estimation

In practical cases, the estimation of P_{NLI} can be affected by various errors, either for fundamental reasons (inaccuracy of the GN-model itself) or because approximations are made to ease its computation. These errors influence the non-linear SNR and ultimately affect system performance assessment. It is therefore important to investigate how sensitive the main system performance indicators are to such errors.

As a case-study example, we concentrate on the determination of an important system parameter: the optimum per-channel launch power, that is, the value of P_{ch} which maximizes SNR_{NL} . We assume equally-spaced channels, all with same format, symbol rate and launch power. In this case the dependence of P_{NLI} on P_{ch} is as follows:

$$P_{\text{NLI}} = \eta P_{\text{ch}}^3 \quad (27)$$

where η is independent of P_{ch} . This is easily seen by observing that the only launch-power dependent quantity in the GNRF is the transmitted signal spectrum $G_{\text{WDM}}(f)$, which can be re-written as:

$$G_{\text{WDM}}(f) = g_{\text{WDM}}(f) \cdot P_{\text{ch}}$$

where $g_{\text{WDM}}(f)$ is assumed to be normalized so that it is independent of P_{ch} . By substituting $G_{\text{WDM}}(f)$ with $[g_{\text{WDM}}(f) \cdot P_{\text{ch}}]$ into the GNRF, a factor P_{ch}^3 is brought into

evidence, whereas the rest of the equation yields the power-independent coefficient η . As a result, we can write:

$$\text{SNR}_{\text{NL}} = \frac{P_{\text{ch}}}{P_{\text{ASE}} + \eta \cdot P_{\text{ch}}^3} \quad (28)$$

Elementary calculus then shows that the optimum launch power is:

$$P_{\text{ch}}^{\text{opt}} = \sqrt[3]{\frac{P_{\text{ASE}}}{2\eta}} \quad (29)$$

We now assume that we do not know η exactly. Rather, we use an approximation η_{app} which bears an error. Characterizing such error as:

$$\Delta\eta_{\text{dB}} = 10 \log_{10}(\eta_{\text{app}}/\eta)$$

and similarly expressing the resulting error on $\Delta P_{\text{ch}}^{\text{opt}}$ as:

$$\Delta P_{\text{ch,dB}}^{\text{opt}} = 10 \log_{10}(P_{\text{ch}}^{\text{opt}}(\eta_{\text{app}})/P_{\text{ch}}^{\text{opt}}(\eta))$$

then from Eq. (29) we easily find:

$$\Delta P_{\text{ch,dB}}^{\text{opt}} = -\frac{1}{3} \Delta\eta_{\text{dB}} \quad (30)$$

This result is important because it shows that the impact of possible inaccuracy in the estimation of NLI is quite substantially ‘dampened’: a 1 dB error in η results in only 1/3 dB error on $P_{\text{ch}}^{\text{opt}}$. A similar behavior is found for the maximum system reach (MSR). Defining the error over the maximum reachable number of spans N_s^{max} as:

$$\Delta N_{s,\text{dB}}^{\text{max}} = 10 \log_{10}(N_s^{\text{max}}(\eta_{\text{app}})/N_s^{\text{max}}(\eta)) \quad (31)$$

then it turns out:

$$\Delta N_{s,\text{dB}}^{\text{max}} \approx -\frac{1}{3} \Delta\eta_{\text{dB}} \quad (32)$$

Another important system parameter that has a similarly dampened dependence on NLI estimation errors is the maximum achievable OSNR at a constant number of spans:

$$\Delta \text{OSNR}_{\text{dB}}^{\text{max}} \approx -\frac{1}{3} \Delta\eta_{\text{dB}} \quad (33)$$

See Sect. VII, and [36] Sect. XII for more details.

As a consequence, from a practical engineering viewpoint, there is substantial tolerance in the amount of NLI estimation error which can typically be accepted. This margin of tolerable error is quite beneficial as it permits to safely use various approximations which are very effective in slashing the GNRF computational complexity. One of them is indeed the LWN approximation introduced in Sect. IV, which is discussed below.

B. NLI spectra and the LWN approximation

In this section we show some examples of actual NLI spectra and then analyze in detail the LWN approximation.

We first focus on a WDM system consisting of 11 channels operating at 32 GBaud. Their power spectrum is assumed raised-cosine with roll-off equal to 0.3. The frequency spacing is 50 GHz. Spans are identical and span loss is exactly compensated for by an EDFA following each span. The other relevant system data are: $N_s=20$, $L_s=100$ km, SMF fiber

with $\alpha=0.2$ dB/km, $\beta_2=20.7$ ps²/km, equivalent to $D=16.5$ ps/(nm·km), and $\gamma=1.3$ 1/(W·km).

In Fig. 3, top, we plot the transmitted signal spectrum $G_{\text{WDM}}(f)$ and the resulting NLI PSD $G_{\text{NLI}}(f)$. A prominent feature of the plot is that NLI appears to be present where the signal is present. Outside of the channel spectra, $G_{\text{NLI}}(f)$ drops off quite rapidly. Expectedly, NLI peaks at the center of the center channel, which is also the most impacted channel of all. A zoomed-in version of the same plot, picturing just the center channel, is reported in Fig. 3, bottom. It shows that $G_{\text{NLI}}(f)$ follows closely the shape of the signal spectrum, albeit with a somewhat enhanced roll-off. Clearly, $G_{\text{NLI}}(f)$ is not flat, although it is not too far from flat over the bandwidth of the channel.

Over the center channel, $G_{\text{NLI}}(f)$ tends to become increasingly flat when channel spacing is reduced. In the limiting case of Nyquist-WDM, it flattens out completely. In Fig. 4, $G_{\text{NLI}}(f)$ is shown for the case of an ideal Nyquist-WDM system, consisting of 17 channels operating at 32 GBaud, each with perfectly rectangular spectrum, with spacing equal to the symbol rate. As a result, the transmitted signal spectrum $G_{\text{WDM}}(f)$ appears as a single wide rectangle. All other data are identical to the previously analyzed system. The figure shows that the PSD of NLI is indeed flat over the center channel, which is again the most impacted.

The resulting spectral shape of NLI in the two cases above suggests that the LWN approximation would generate no appreciable error in the estimation of P_{NLI} for the center channel in the case of Nyquist-WDM, whereas some error would be incurred in the 50 GHz spaced system.

In the following we show the results of a study of such error, over a wide range of channel count and channel spacing. The system parameters were: 32 GBaud, raised-cosine PSD, roll-off 0.02, SMF fiber, identical spans with $N_s=25$, $L_s=85$ km, span loss exactly compensated for by EDFAs. The Rx equalizer is assumed to implement a transfer function matched to the signal and, as a result, $|H_{\text{Rx}}(f)|^2$ has the same shape as the signal average PSD. The P_{NLI} estimation error on the center channel of the comb, due to the LWN approximation, was characterized as:

$$\Delta P_{\text{NLI,dB}} = 10 \log_{10} \left(P_{\text{NLI}}^{\text{LWN}} / P_{\text{NLI}} \right) \quad (34)$$

where P_{NLI} is calculated as Eq. (24) and $P_{\text{NLI}}^{\text{LWN}}$ is calculated as Eq. (26). The results are shown in Fig. 5 vs. channel spacing Δf_{ch} and for a number of channels N_{ch} ranging between 1 and 25. The figure shows that the absolute maximum value of $\Delta P_{\text{NLI,dB}}$ is found, expectedly, for a single channel, and amounts to about 0.53 dB. At 5 channels, it does not exceed 0.4 dB even for 50 GHz spacing. For 25 channels it drops below 0.35 dB for $\Delta f_{\text{ch}}=50$ GHz and below 0.25 dB $\Delta f_{\text{ch}} < 38$ GHz. Note that these errors are all *biased positive*, that is P_{NLI} is slightly *overestimated*.

In conclusion, in practical WDM systems the LWN approximation causes small errors in P_{NLI} estimation, whose impact on the main system performance indicators is almost negligible due to the attenuation effect highlighted in Sect. IV-A. In any case, they lead to conservative predictions, i.e., to a slight performance *underestimation*.

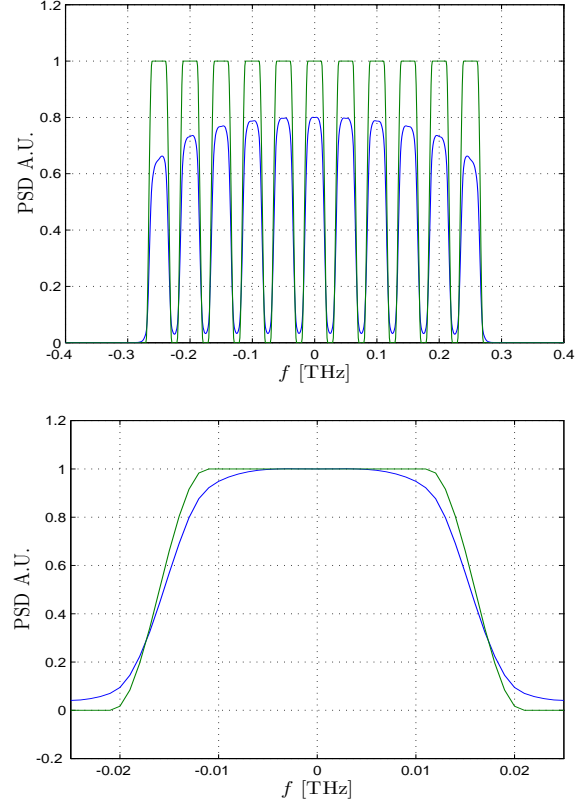


Fig. 3. Top plot: green solid line: PSD of the transmitted signal $G_{\text{WDM}}(f)$, equivalent to 11 channels at 32 GBaud; blue solid line: PSD of NLI noise $G_{\text{NLI}}(f)$ after 20 spans of 100 km of SMF. Bottom plot, same as top, zoomed in on the center channel. Signal and NLI spectra arbitrarily re-scaled in each plot for ease of comparison.

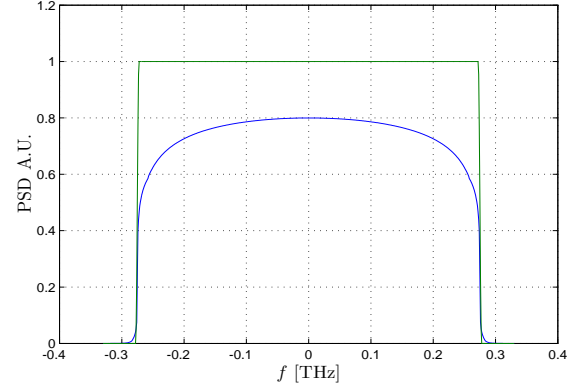


Fig. 4. Green solid line: PSD of the transmitted signal $G_{\text{WDM}}(f)$, equivalent to 17 Nyquist-WDM channels at 32 GBaud. Blue solid line: PSD of NLI noise $G_{\text{NLI}}(f)$ after 20 spans of 100 km of SMF. Spectra arbitrarily re-scaled for ease of comparison.

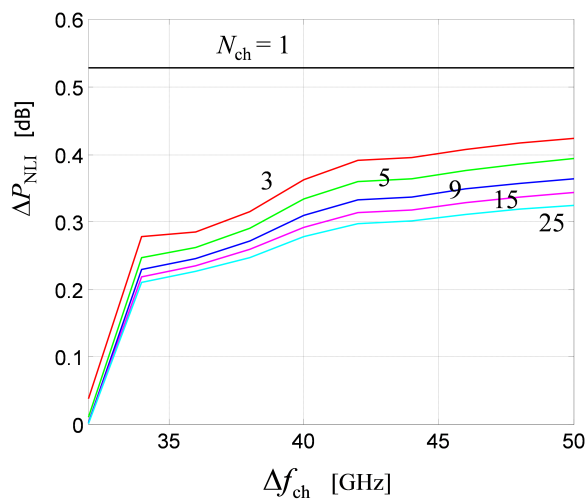


Fig. 5. Plot of the NLI estimation error ΔP_{NLI} in dB, on the center channel of a WDM comb, due to the LWN approximation, vs. channel spacing Δf_{ch} , for a number of channels N_{ch} ranging from 1 to 25, after 25 spans of SMF.

V. GN AND IGN MODEL VALIDATION

The validation of the GN or IGN-model requires benchmark-grade reliable results to compare it with. These benchmarks can be built based on either simulations or experiments. Although, ultimately, it is adherence to physical reality what really matters, experiment-based validations are somewhat problematic. They are typically limited in scope, because it is hard to carry them out over a large number of system configurations. In addition, measurement uncertainties may be significant. Nonetheless, a few GN-model validation experiments have been attempted, yielding good agreement between predictions and results [58]-[59]. They will be discussed in Sect. VII. In addition, experiments not explicitly designed for GN-model validation appear to agree well with GN-model predictions [76], [77], too.

In this section, however, we choose to concentrate on validation based on a simulative approach, to be able to address a wide range of system configurations. Such an approach can be considered reliable, provided that two key conditions are met. First, the NLSE/ME integration procedure must be trusted and verified: we relied on an extensively tested split-step algorithm with controlled accuracy parameters. Secondly, simulated signal transmission must occur with sufficient statistical diversity so that Monte-Carlo averaging can produce reliable results. To this end, we used all independent PRBSs on all channels. We also imposed adequate PRBS length and overall simulation length.

This section is divided into two parts: in the first part we compare the GN and IGN-model predictions of maximum system reach (MSR) with simulations carried out over a very broad range of system configurations. This effort provides a first overall assessment of the model performance.

In the second part, we investigate in depth some of the accuracy issues that emerge from the first part. We specifically address the GN and IGN model assumptions introduced in Sect. II-A, trying to assess to what extent each one of them is verified and which one of them may cause the errors observed

Fiber	α [dB/km]	D [ps/nm/km]	γ [1/W/km]
PSCF	0.17	20.1	0.8
SMF	0.2	16.7	1.3
NZDSF	0.22	3.8	1.5

TABLE I
PARAMETERS OF THE THREE FIBER TYPES USED IN SECTION V-A.

in the first part of the section.

A. Broad-range simulative validation

As test-setups we concentrated on systems based on PM-QPSK, PM-16QAM and PM-64QAM. At the Tx, digital pre-filtering was applied to obtain pulses with a square-root-raised-cosine spectrum, with roll-off equal to 0.05. Then, four ideal DACs generated the electrical signals driving two nested Mach-Zehnder modulators, operated in their linear trans-characteristic range. The symbol rate (R_s) was set to the typical industry standard value of 32 GBaud. The channel spacing Δf_{ch} spanned the following values: 33.6, 35, 40, 45, 50 GHz. The lowest value, corresponding to $1.05 \cdot R_s$ is the minimum spacing still ensuring no inter-channel linear crosstalk, given the chosen roll-off. The number of transmitted WDM channels was set to 15. Data were generated using multiple independent PRBS's of length $(2^{16} - 1)$, four for each PM-QPSK channel, eight for each PM-16QAM channel and twelve for each PM-64QAM channel. PRBSs were different from channel to channel. The simulation length was 2^{17} symbols. These lengths were tested as to their ability to ensure sufficient Monte-Carlo diversity.

Three fiber types were employed, whose parameters are reported in Table I. They are typical of SMFs, large-effective-area PSCFs and NZDSFs. Overall, they cover a broad variety of dispersions, attenuations and non-linearity coefficients. The UT test links were homogenous and transparent, with lumped EDFA amplification. The EDFA noise figure was 5 dB.

Channel selection was performed at the Rx by properly tuning the local oscillator. After balanced photo-detection, an electrical anti-alias filter of Bessel type (5 poles) with bandwidth $R_s/2$ was inserted. Its output was sampled at 2 samples per symbol. Then, electronic CD compensation was performed, followed by polarization de-multiplexing and equalization, by means of an adaptive 2x2 equalizer, driven by a decision-directed least-mean-square algorithm. Carrier and phase recovery were not needed since the Tx and local-oscillator lasers of the center channel were assumed ideal (no phase noise). All other channels were transmitted with 5 MHz linewidth, to obtain some phase scrambling in the comb.

This validation effort focused on comparing the maximum system reach (MSR) found through simulations with the model prediction. By 'MSR' we mean the following. We define the system reach (SR) as the maximum number of spans that can be achieved while BER is below a set target, given a certain launch power. The MSR is the highest value of SR vs. launch power, i.e., it is the SR which is obtained using the *optimum* launch power.

We assumed the systems to operate with a FEC whose BER threshold is equal to 10^{-2} . For the sake of realism, however,

we did not aim at the FEC BER threshold. Instead, we aimed at a target BER which corresponds to the FEC threshold derated by 2 dB of SNR, considered as a realistic system margin. The resulting target BERs were: PM-QPSK, $1.70 \cdot 10^{-3}$; PM-16QAM, $2.04 \cdot 10^{-3}$; PM-64QAM, $2.82 \cdot 10^{-3}$. These BERs are different because of the different slope of the BER-vs.-SNR curves of each format. In order to aim at a reasonable number of spans with all formats and fibers, i.e., neither too large nor too small, the span length was set to a different value, depending on format: 120, 85 and 50 km, for PM-QPSK, PM-16QAM and PM-64QAM, respectively.

A parallel set of simulations was also performed with identical set-ups, except the transmitted signals were guaranteed to adhere to the signal-Gaussianity assumption through the application of very substantial pre-dispersion (PD) before launch into the fiber (100,000 ps/nm).

As previously mentioned, the simulations were based on the split-step algorithm, which is known to produce various artifacts, among which spurious FWM. We applied a logarithmic step law [60], to mitigate it. To constrain the minimum step size, we imposed both a spurious FWM suppression of 50 dB [60] and a maximum non-linear phase shift, due to the total WDM instantaneous power integrated over a 5 ps time-window, not exceeding 0.1 radians. We chose these numbers by verifying that further tightening of these accuracy constraints would not change the simulation results.

The plots of the MSR for each set-up are shown in Fig. 6, where markers are simulation results (circles for non-PD signals and squares for PD signals) and solid lines are obtained through numerical integration of either the GNRF Eq. (2) or the IGNRF Eq. (11). The overall set of necessary simulations took about 1 year of CPU time. The numerical integration of the GNRF and IGNRF, performed using interpreted Matlab code, took about 10 hours, overall.

The prominent feature of the plots is that the PD simulations are very close to the GN-model predictions, within 0.25 dB error for all formats, fibers and spacings, a value comparable with the residual uncertainty of the simulations. These results suggest that the accuracy of the GN-model is excellent, when the signal-Gaussianity assumption is well verified. This in turn strongly suggests that also the perturbation and AGN assumptions, mentioned in Sect. II-A, must be verified to a sufficient extent, at least at the optimum launch power corresponding to the MSR.

When PD is removed and the systems undergo what we call the ‘initial dispersion transient’ (IDT), during which approximate signal Gaussianity is only gradually approached, then a greater amount of error is found between the GN-model and simulations. Still, the error never exceeds 0.8 dB on the MSR across all system configurations. In addition, the GN-model appears to have the interesting feature of being always *conservative* for non-PD signals, that is it predicts a slightly *lower* MSR than the simulations show.

It is also interesting to remark that for non-PD signals the IGN-model appears to systematically yield substantially more accurate predictions than the GN-model, in agreement with what had been found in a prior validation effort [34]. This result is somewhat puzzling, because the IGN-model is

a more approximate model than the GN-model. So, at least in principle, one could expect a somewhat greater error from the IGN than from the GN-model.

The specific features of the GN and IGN-model errors that emerge from Fig. 6 are investigated in detail in the next section. Already at this stage, however, it can be argued that both the GN and IGN-model appear to effectively capture the general features of the system impact of non-linear propagation, across a very wide range of systems and set-ups, within rather small error brackets.

B. The perturbative and AGN assumptions

If the perturbative or the AGN assumptions failed, substantial error would show up in the comparison of the GN-model with PD-signal simulations, where the signal-Gaussianity assumption is certainly very well verified. Instead, the results of the previous section show excellent agreement in this case. This suggests that major inaccuracy of either the perturbative or the AGN assumptions should be ruled out.

As a further specific test of the AGN assumption, in the shown system simulations we both measured BER through Monte-Carlo direct error count and we also calculated it by means of the canonical BER formulas, using as SNR the one directly measured over the signal constellation, averaged over all signal points. If the statistical features of NLI departed substantially from AGN, then the analytical formulas, which are derived based on the AGN assumption, would produce BER results different from the Monte-Carlo ones. Instead, the agreement between the two BER values was always very good. This shows that, *at least from the viewpoint of practical system performance evaluation*, the AGN assumption can be considered effective. This conclusion matches the one reached in prior simulative and experimental papers which specifically investigated this issue [34], [61]-[63].

C. The signal-Gaussianity assumption and the IDT

The fact that the GN-model shows almost no error with PD signals, whereas some error is present with non-PD signals, strongly suggests that it is the signal-Gaussianity assumption that at least partially *fails* in the latter case and needs to be carefully investigated.

To carry out a specific study² dealing with the of the signal-Gaussianity assumption, we concentrated on the direct evaluation of NLI, rather than on the estimation of system-related performance parameters. The reason is that the latter typically ‘masks’ or ‘dampens’ the errors on NLI estimation, as discussed in Sect. IV-A. The same simulated test formats and set-ups described in the previous section were used, with a few minor differences. The Tx spectrum roll-off was set to 0.02 and only one spacing was used: $\Delta f_{\text{ch}}=33.6$ GHz, that is $1.05 \cdot R_s$. The PRBS length was boosted to $(2^{18} - 1)$ and the

²The following study on NLI generation and accumulation was preliminarily reported on at ECOC 2013 as [66]. At the same conference, another paper was presented on similar topics [67]. These two papers have later been followed by [50]-[51], where the errors due to the GN-model assumptions are also dealt with. As stated in a previous footnote, these developments are too recent to be discussed in this paper.

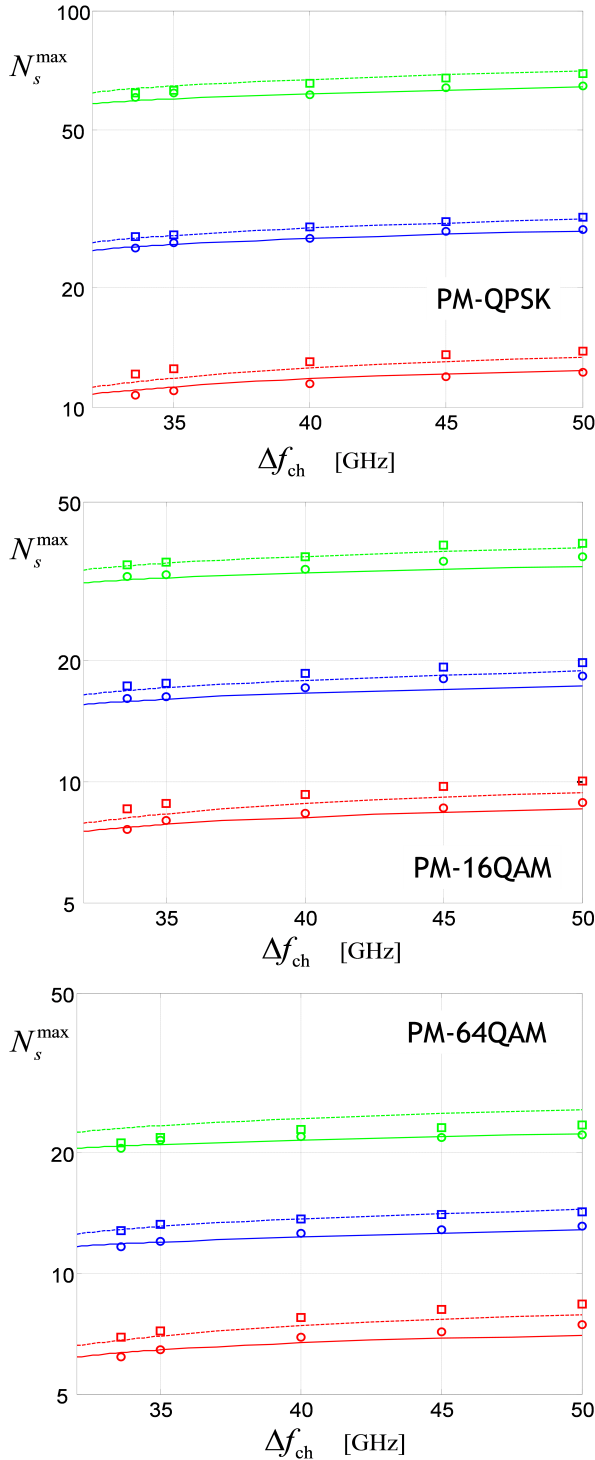


Fig. 6. Plot of maximum system reach (MSR) in number of spans N_s^{\max} for the test set-ups, vs. channel spacing Δf_{ch} . Top: PM-QPSK; middle: PM-16QAM; bottom PM-64QAM. Span lengths: 120, 85 and 50 km, respectively. Red items: NZDSF. Blue items: SMF. Green items: PSCF. Solid lines: GN-model predictions. Dashed lines: IGN-model predictions. Circles: simulations with pre-dispersion. Squares: simulations without pre-dispersion.

total simulation lengths was increased also to 2^{18} symbols. The number of simulated channels was 9. Here too, both conventional and PD signals (200,000 ps/nm pre-dispersion) were launched. The span length was set to 100 km for all set-ups. Regarding the split-step parameters, the spurious FWM suppression was set to 50 dB and the maximum non-linear phase shift was tightened to 0.025 radians.

ASE noise was turned off so that the Rx signal disturbance was due only to NLI. The estimation of the NLI variance was performed on the center channel, as follows. The Rx electrical noise variance of each signal point of the constellation was evaluated on both quadratures and polarizations. The results were averaged to obtain a single variance value σ_{tot}^2 . The same simulation was then repeated with fiber non-linearity turned off, all other parameters identical, producing an estimate of possible residual disturbance in linearity σ_{lin}^2 . Then, the NLI variance was calculated as:

$$\sigma_{\text{NLI}}^2 = \sigma_{\text{tot}}^2 - \sigma_{\text{lin}}^2 \quad (35)$$

Note that, ideally, $\sigma_{\text{lin}}^2=0$, since both NLI and ASE were turned off. However, we found that σ_{lin}^2 was never exactly zero, possibly reflecting some minor inter-symbol interference, so that subtracting σ_{lin}^2 was necessary for accurate σ_{NLI}^2 estimation. The quantity P_{NLI} can then be found from σ_{NLI}^2 because they are related through a constant:

$$P_{\text{NLI}} = \frac{R_s}{B_H} \sigma_{\text{NLI}}^2$$

where B_H is given by Eq. (25). For each system set-up, P_{NLI} was measured after each span, from 1 to 50 spans.

As pointed out in Sect. IV-A, NLI is such that $P_{\text{NLI}} \propto P_{\text{ch}}^3$, where P_{ch} is the launch power per channel. Hence, we focused on the quantity $\eta = P_{\text{NLI}}/P_{\text{ch}}^3$, because it is theoretically independent of P_{ch} . All simulations were performed with a relatively low value of P_{ch} of -6 dBm to ease the burden of the integration algorithm and suppress any possible error due to the perturbation assumption.

In Fig. 7-(top), η is plotted vs. the number of spans N_s for PM-QPSK over SMF. The dashed line represents the calculated result based on the GN-model, the dashed-dotted line based on the IGN-model. The solid lines are η from simulations, without PD (red curve) and with PD (blue curve). The PD simulation results are in excellent agreement with the GN-model. In contrast, the non-PD simulations show about 6 dB less NLI noise produced over the first span than either the PD simulation or the GN-model predict. The difference then decreases steadily. A similar picture emerges when considering PM-16QAM, Fig. 7-(center), although discrepancies are less pronounced. The first-span gap is 3.5 dB rather than 6 and, in general, the non-PD and PD simulations run closer. Again, the PD results are in very good agreement with the GN-model.

In Fig. 7-(bottom) we show the result for PM-QPSK over NZDSF. Despite the lower fiber CD, which certainly slows down the IDT, the results are not substantially different from PM-QPSK over SMF. The gap after 1 span is smaller (4 dB vs. 6 dB). On the other hand, convergence of non-PD to PD is somewhat slower.

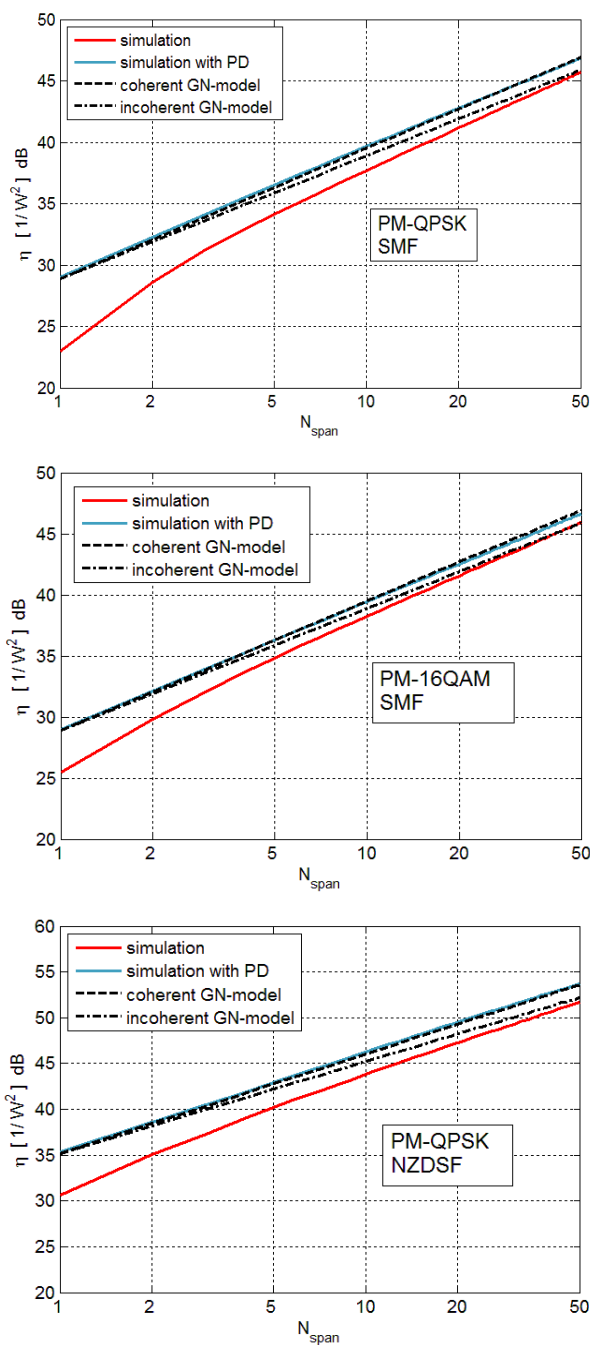


Fig. 7. Normalized NLI noise variance η vs. the number of spans N_{span} , over the center channel of 9 WDM channels, with 100 km span length. Solid lines: simulations, red without pre-dispersion, blue with pre-dispersion (PD). Dashed lines: GN-model. Dash-dotted lines: IGN-model.

The NLI results of Fig. 7 shed light on the MSR results of Fig. 6. The very good adherence of the GN-model to the PD-signal behavior is confirmed at the fundamental level of η . As for non-PD signals, the error seen in Fig. 6 is clearly due to the GN-model overestimating NLI generation especially in the first spans, when the signal statistical distribution is farther from Gaussian. Overestimating NLI leads to always underestimating the MSR, which is what is consistently seen in Fig. 6. In other words, the GN-model confirms its being *always conservative*.

Although the error between the GN-model prediction and the simulated η of conventional signals is substantial, especially in the first spans, its actual impact on system performance prediction is limited, as shown in Fig. 6, due to the circumstances highlighted in Sect. IV-A. In fact, considering for instance PM-QPSK over SMF at 33.6 GHz spacing in Fig. 6, the error on the MSR, defined as $\Delta N_{s,\text{dB}}^{\text{max}}$ in Eq. (31), is only 0.3 dB. The corresponding error on η from Fig. 7 is about 1 dB, which confirms the ‘dampening’ by approximately a factor 1/3 in dB, as pointed out in Sect. IV-A. This strong attenuation of the impact of NLI estimation errors when assessing system performance indicators will be further discussed in Sect. VII.

D. Interpreting the results

A tentative interpretation of the smaller NLI generation by conventional signals than by PD signals, seen in Fig. 7, can be based on the conjecture that the amount of NLI produced somehow depends on the extent of the signal instantaneous power variations. This hypothesis is supported by some of the results shown for instance in [44]. Indeed, conventional signals have smaller power variations in the first spans than the Gaussian-distributed PD signals. Therefore, the above conjecture would predict that conventional signals should produce less NLI in the first spans than the PD ones, as in fact happens.

Then, as the IDT progresses, and the conventional signals distribution tend to gradually become closer to Gaussian, the amount of NLI generated by conventional and PD signals would tend to converge. As a result, the non-PD η curve would tend towards the PD curve, and to what is predicted by the GN-model. Such general behavior is in fact found in Fig. 7.

This tentative interpretation is qualitatively supported by the evolution of a parameter that quantifies the single-channel instantaneous power variations. It is:

$$\Theta(z) = 2 \frac{\langle P_{\text{ch}}^2(t) - \bar{P}_{\text{ch}}^2 \rangle}{\bar{P}_{\text{ch}}^2}$$

where $P_{\text{ch}}(t)$ is the instantaneous power of the channel, \bar{P}_{ch} is its average power and the symbol $\langle \cdot \rangle$ means time-average. If the signal has no power variations, then $\Theta=0$. If instead the signal field components are Gaussian-distributed, then $\Theta=1$.

In Fig. 8, Θ is plotted vs. the propagation distance z , for a single PM-QPSK channel with raised-cosine PSD and roll-off 0.02, over SMF, in linearity. The solid line is from simulation. It agrees well with the analytical formula (dashed line), valid for small roll-off:

$$\Theta(z) = 1 - 2 [1 - \Theta(0)] \frac{\cos(\mu z) + (\mu z) \cdot \text{sinint}(\mu z) - 1}{\mu^2 z^2} \quad (36)$$

where ‘sinint’ is the sine-integral function and $\mu = 4\pi\beta_2 R_s^2$.

The figure shows that Θ starts at the low level $\Theta(0)=0.308$. This initial value depends both on format and roll-off. Then it gradually goes up, with a trend towards saturating at 1, as expected.

This trend appears to qualitatively agree with what is seen in Fig. 7. However, the underlying phenomenon is certainly more complex than described by just $\Theta(z)$. Nonetheless, this

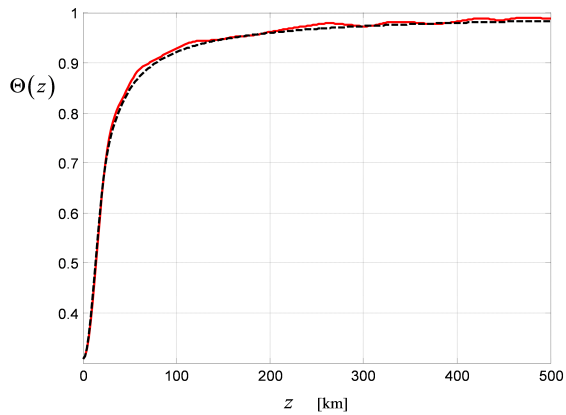


Fig. 8. Plot of the power-variation parameter $\Theta(z)$ for a PM-QPSK channel with raised-cosine spectrum, roll-off 0.05, over SMF, in linearity. Solid red line: simulation. Black dashed line: Eq. (36). A value of 1 corresponds to a signal with Gaussian distribution.

approach could be a starting point for trying to obtain a low-complexity (perhaps approximate) GN-model correction that could account for the IDT.

E. IGN-model errors

The IGN-model is identical to the GN-model, except for one additional approximation, i.e., that NLI accumulation occurs incoherently. Therefore, the IGN-model is more ‘approximate’ than the GN-model, so that one would expect it to be less accurate. Surprisingly, from both Fig. 6 and Fig. 7 it appears that the IGN model is typically *closer* to the simulation results of non-PD signals than the GN-model. In fact, its predictions are quite precise.

Interestingly, the greater accuracy of the IGN-model appears not to be due to a more faithful modeling of signal propagation at a fundamental level, but to the following circumstance. The signal-Gaussianity assumption leads to overestimating NLI, while the incoherent accumulation approximation leads to underestimating it. Therefore, these two approximations, which are both present in the IGN-model, tend to cancel each other’s error out. Paradoxically, the GN-model, which uses only the first of the two, does not benefit from this cancellation.

Accidental as it may be, the accuracy of the IGN-model is a useful result, since the IGN-model appears to be quite adequate for studying a wide range of practical scenarios, as shown for instance by Fig. 6, while it is much easier to handle than the GN-model, both analytically and numerically.

VI. ANALYTICAL CLOSED-FORM RESULTS

In general, the GNRF cannot be solved analytically. However, useful closed-form approximate solutions can be derived, which can be of help in carrying out preliminary performance assessments, or be the basis for real-time, physical-layer awareness computation for flexible wavelength-routed networks. In this section we collect a selection of these results. For each one of them we point out the assumptions made to derive them and the range of validity of the results. Derivations will not be reported here. Unless otherwise specified, they can be found in [36].

To make the analytical derivations possible, all of the following formulas disregard the dispersion derivative β_3 . On the other hand, the impact of β_3 is typically negligible [38]. It may start to be felt for $\beta_2 < 2$ depending on system parameters. However, for very low β_2 , the issue of the IDT becomes important as well (see Sect. V-C). For either reason, the following formulas should not be used for very low values of dispersion.

Apart from the above remark, when ‘accuracy’ or ‘errors’ are mentioned in this section, they are referred to how well the closed-form formulas approximate the GNRF. They are not referred to how well the model in general approximates simulations or real systems, a topic that was dealt with in Sect. V. We also remind the reader that the errors incurred by the formulas in estimating NLI is substantially ‘attenuated’ when system performance indicators are computed, as pointed out in Sect. IV-A.

Some of these closed-form formulas will be exploited in Sect. VII to obtain simple system ‘design rules’.

A. Ideal Nyquist-WDM over a single span

By ‘ideal Nyquist-WDM’ we mean a system whereby each channel has a perfectly rectangular spectrum of width equal to R_s and the channel spacing also coincides with R_s .

Over a single span, assuming transparency, with lumped amplification at the end, an approximate solution to the GNRF, at the frequency $f=0$ conventionally corresponding to the center of the overall Nyquist-WDM comb, is:

$$G_{\text{NLI}}^{1 \text{ span}}(0) \approx \frac{8}{27} \gamma^2 G_{\text{WDM}}^3 L_{\text{eff}}^2 \frac{\text{asinh}\left(\frac{\pi^2}{2} |\beta_2| L_{\text{eff,a}} B_{\text{WDM}}^2\right)}{\pi |\beta_2| L_{\text{eff,a}}} \quad (37)$$

where ‘asinh’ is the hyperbolic arcsin function, $L_{\text{eff,a}}=1/2\alpha$ is the asymptotic effective length and G_{WDM} is the value of the (flat) PSD of the signal. Note that $\text{asinh}(x) \approx \log_e(2x)$ when $x > 3.5$, with a relative error of less than 1%. Formulas similar to Eq. (37) can be found in some of the papers dealing with perturbative models discussed in Sect. II-B, such as [28], [29], [31], [33], [41] and others.

To derive Eq. (37) the following approximation is necessary within the integrand of the GNRF:

$$|1 - e^{-2\alpha L_s} e^{j4\pi^2 \beta_2 L_s f_1 f_2}|^2 \approx 1 \quad (38)$$

where f_1 and f_2 are the integration variables. This approximation causes negligible loss of accuracy if the span loss is greater than about 10 dB. If so, Eq. (37) is very accurate, with a maximum error of about 0.35 dB occurring at $x \approx 1$, where x is the overall argument of the asinh function. Note that for an SMF-based system with $L_s=100$ km, $x = 1$ corresponds to a very small value $B_{\text{WDM}}=20$ GHz. When $x > 10$ the error is below 0.1 dB and asymptotically tends to 0.

Recently, variations to this formula were proposed in order to reduce the error occurring at low x values, based on analytical arguments [57]. Heuristically, one way to bring its maximum error below 0.1 dB for *all* values of x is to replace $\pi^2/2$ in the asinh argument with the constant 4.6. This way, accuracy is gained at low x , while the error grows somewhat for high values of x , but always stays below 0.1 dB.

We assume that the span is transparent, with lumped amplification at the end, and that all channels are identical. We define B_{ch} as the -3dB bandwidth of each channel and Δf as the channel spacing. Then, the NLI PSD at the center of the center channel is approximately:

$$G_{\text{NLI}}^{\text{1 span}}(0) \approx \frac{\gamma^2 G_{\text{WDM}}^3 L_{\text{eff}}^2 (\frac{2}{3})^3}{\pi |\beta_2| L_{\text{eff},a}} \cdot \left\{ \begin{aligned} & \sum_{k=-(N_{\text{ch}}-1)/2}^{(N_{\text{ch}}-1)/2} [\text{asinh}(\pi^2 |\beta_2| L_{\text{eff},a} B_{\text{ch}} [k\Delta f + B_{\text{ch}}/2]) - \\ & \text{asinh}(\pi^2 |\beta_2| L_{\text{eff},a} B_{\text{ch}} [k\Delta f - B_{\text{ch}}/2])] + \\ & \text{asinh}(\frac{1}{2}\pi^2 |\beta_2| L_{\text{eff},a} B_{\text{ch}}^2) \end{aligned} \right\} \quad (39)$$

As for Eq. (37), this formula too relies on the approximation shown in Eq. (38), which starts causing non-negligible error if span loss < 10 dB. The derivation also assumes that the channel spectra are rectangular, so some error is incurred if channels depart significantly from that shape. Assuming large-enough span loss and rectangular spectra, Eq. (39) stays below 0.5 dB of error across all practical parameter values, for any number of channels. If, in addition, R_s (which coincides with B_{ch} for rectangular spectra) is larger than 25 GBaud, the error is even lower, less than 0.3 dB. Going from rectangular spectra to raised-cosine with roll-off 0.3 causes an error increase of up to 0.3 dB, depending on system parameters.

The interesting feature of all the above errors is that they are biased: i.e. they occur in the range 0 to the amount indicated above. As a result, Eq. (39) always overestimates the NLI PSD, i.e., it is conservative.

Eq. (39) can be greatly simplified if $B_{\text{ch}} > 25$ GHz. In that case, through further approximations [36], the following compact formula can be obtained:

$$G_{\text{NLI}}(0) \approx \frac{8}{27} \frac{\gamma^2 G_{\text{WDM}}^3 L_{\text{eff}}^2}{\pi |\beta_2| L_{\text{eff},a}} \text{asinh}\left(\frac{\pi^2}{2} |\beta_2| L_{\text{eff},a} B_{\text{ch}}^2 N_{\text{ch}}^2 \frac{B_{\text{ch}}}{\Delta f}\right) \quad (40)$$

Eq. (40) incurs only about 0.1 dB extra error vs. Eq. (39), provided that $B_{\text{ch}} > 25$ GHz.

In summary, Eqs. (39)-(40) constitute effective tools to assess the non-linearity performance of typical practical modern WDM systems, leading to sufficiently accurate estimates of system performance parameters.

C. Multiple spans

In the case of a homogeneous and transparent link, one can choose to use the IGN-model and then, according to Eq. (15):

$$G_{\text{NLI}}^{\text{inc}}(0) = G_{\text{NLI}}^{\text{1 span}}(0) \cdot N_s$$

where $G_{\text{NLI}}^{\text{inc}}(0)$ can be calculated using either Eq. (37) or Eqs. (39)-(40).

Otherwise, one can chose the GN-model of Eq. (16):

$$G_{\text{NLI}}^{\text{inc}}(0) = G_{\text{NLI}}^{\text{1 span}}(0) \cdot N_s^{1+\epsilon}$$

and in this case the parameter ϵ is needed, for which the following approximate closed-form formula is available for

the ideal Nyquist-WDM case:

$$\epsilon \approx \frac{3}{10} \cdot \log_e \left(1 + \frac{6}{L_s} \frac{L_{\text{eff},a}}{\text{asinh}\left(\frac{\pi^2}{2} |\beta_2| L_{\text{eff},a} B_{\text{WDM}}^2\right)} \right) \quad (41)$$

This formula is quite accurate, within a few percent relative error, provided that the argument of the asinh is greater than 10 and that span loss is greater than 10 dB. For the non-Nyquist case, a coarser approximate formula can be written:

$$\epsilon \approx \frac{3}{10} \cdot \log_e \left(1 + \frac{6}{L_s} \frac{L_{\text{eff},a}}{\text{asinh}\left(\frac{\pi^2}{2} |\beta_2| L_{\text{eff},a} B_{\text{ch}}^2 [N_{\text{ch}}^2 \frac{B_{\text{ch}}}{\Delta f}]\right)} \right)$$

This formula turns out to typically underestimate ϵ by 5% to 20%. Its accuracy is therefore limited, but the main parameter dependencies appear to be correctly captured by it. Note that it should not be used outside of the parameter range of validity of Eq. (40), indicated in Sect. VI-B.

D. The IGN-model-based ‘whole-system-solver’ formula

The homogenous and transparent link assumption made in the previous section is rather unrealistic for typical terrestrial links, where spans can be all different and whose loss may not be exactly compensated for. In addition, channels may have different launch powers, symbol rates and uneven spacing, such as shown in Fig. 9. Moreover, in practical analysis/design problems, it is typically necessary to assess the performance of all channels of the comb, not just the center one.

It is possible to derive a closed-form ‘whole-system-solver’ formula, which can accommodate all the above diversity and features, provided that the IGN-model incoherent accumulation approximation of Eq. (9) is accepted. The formula also makes other simplifying assumptions, such as that channels have approximately rectangular PSD.

The final formula is written as follows:

$$G_{\text{NLI}}(f_{\text{ch},i}) = \frac{16}{27} \sum_{n_s=1}^{N_s} \gamma_{n_s}^2 L_{\text{eff},n_s}^2 \cdot \prod_{k=1}^{n_s-1} \Gamma_k^3 e^{-6\alpha_k L_{s,k}} \cdot \prod_{k=n_s}^{N_s} \Gamma_k e^{-2\alpha_k L_{s,k}} \cdot \sum_{n=1}^{N_{\text{ch}}} G_{\text{ch},n} G_{\text{ch},n} G_{\text{ch},i} \cdot (2 - \delta_{n,i}) \cdot \psi_{n,i,n_s} \quad (42)$$

where: $G_{\text{NLI}}(f_{\text{ch},i})$ is the NLI PSD at the center frequency $f_{\text{ch},i}$ of the i -th channel of the comb; $G_{\text{ch},i}$ is the PSD of the transmitted signal at the center frequency of the i -th channel; $\delta_{n,i}$ is Kronecker’s delta, i.e., it is one if $n=i$ and zero otherwise; finally, ψ is:

$$\psi_{n,i,n_s} \approx \frac{\text{asinh}(\pi^2 [2\alpha_{n_s}]^{-1} |\beta_{2,n_s}| |f_{\text{ch},n} - f_{\text{ch},i} + B_{\text{ch},n}/2| B_{\text{ch},i})}{4\pi (2\alpha_{n_s})^{-1} |\beta_{2,n_s}|} - \frac{\text{asinh}(\pi^2 [2\alpha_{n_s}]^{-1} |\beta_{2,n_s}| |f_{\text{ch},n} - f_{\text{ch},i} - B_{\text{ch},n}/2| B_{\text{ch},i})}{4\pi (2\alpha_{n_s})^{-1} |\beta_{2,n_s}|}, \quad n \neq i \quad (43)$$

$$\psi_{i,i,n_s} \approx \frac{\text{asinh}\left(\frac{\pi^2}{2} |\beta_{2,n_s}| [2\alpha_{n_s}]^{-1} B_{\text{ch},i}^2\right)}{2\pi |\beta_{2,n_s}| [2\alpha_{n_s}]^{-1}}, \quad n = i \quad (44)$$

where $B_{\text{ch},i}$ is the -3dB bandwidth of the i -th channel.

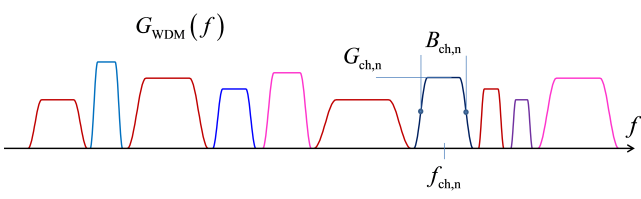


Fig. 9. Example of a possible WDM comb with unequal channel bandwidth, unequal channel flat-top PSD and uneven spacing.

Despite the many approximations, this formula still provides reasonably reliable results, typically to within 1.5 dB accuracy vs. the GNRF, provided that channel spectra are at least approximately flat-top, such as raised-cosine. Even though a 1.5 dB error is per se a rather large number, its impact on, for instance, the system maximum reach would only be 0.5 dB (see Sect. IV-A), so that as a preliminary coarse estimation tool, Eqs. (42)-(44) may be quite effective.

E. Nyquist-WDM with distributed amplification

No analytical closed-form formulas are currently available solving the GNRF or IGNERF in the presence of distributed Raman amplification. Partial results providing the FWM efficiency ρ with Raman can be found in [35], [36].

When the signal is ideal Nyquist-WDM and amplification is ideally distributed, that is $g(z) = \alpha$, then the following rather accurate formula can be obtained:

$$G_{\text{NLI}}(0) \approx \frac{16}{27} \gamma^2 G_{\text{WDM}}^3 L_{\text{tot}} \frac{\text{asinh}\left(\frac{1}{3} \pi^2 |\beta_2| L_{\text{tot}} B_{\text{WDM}}^2\right)}{\pi |\beta_2|} \quad (45)$$

An even more accurate formula is shown in [36], App. I, which, however, contains a special function. Eq. (45) is found by replacing such special function with a suitable approximation.

Note that in this case the concept of ‘span’ loses meaning: the fiber is homogeneous and transparent from the beginning to the end of the link. Therefore, this formula directly provides the NLI PSD due to the entire link, of length L_{tot} , according to the GN-model (coherent NLI accumulation). Eq. (45) is accurate to within 0.1 dB if the argument of the asinh is >25 . For a 1,000 km link over SMF, this condition is already met if $B_{\text{WDM}} > 20$ GHz.

Although physically unrealistic, the case of ideal distributed amplification represents the theoretically best-performing amplification scheme and therefore provides a sort of upper-bound to the potential performance of all possible distributed amplification solutions. Eq. (45) will be used in Sect. VIII to derive non-linear link throughput estimates.

VII. DESIGN RULES FOR REACH MAXIMIZATION IN UNCOMPENSATED LINKS

In this section we address the problem of finding simple closed-form formulas that provide effective ‘design rules’ for UT systems. In particular, we are interested in pointing out the *variational* dependence of the MSR vs. the main system parameters. In other words, we want to find simple expressions

showing how much MSR is lost or gained vs. any change in the main system parameters.

We concentrate on transparent and homogenous links, with lumped (EDFA) amplification and all identical equispaced channels. We look at the performance of the center channel of the comb, which was shown in Sect. IV-B to be the most impacted by NLI. We adopt the LWN assumption, so that P_{NLI} in the SNR_{NL} can be calculated, using Eq. (26), as:

$$P_{\text{NLI}} = G_{\text{NLI}} \cdot R_s \quad (46)$$

where G_{NLI} indicates $G_{\text{NLI}}(f)$ evaluated at the center frequency of the center channel. We then assume incoherent accumulation (the IGN-model) so that we have:

$$G_{\text{NLI}} = G_{\text{NLI}}^{1 \text{ span}} \cdot N_s \quad (47)$$

Combining Eqs. (46) and (47) we can write:

$$P_{\text{NLI}} = P_{\text{NLI}}^{1 \text{ span}} \cdot N_s \quad (48)$$

having defined:

$$P_{\text{NLI}}^{1 \text{ span}} = G_{\text{NLI}}^{1 \text{ span}} \cdot R_s \quad (49)$$

As a result SNR_{NL} can be written as:

$$\text{SNR}_{\text{NL}} = \frac{P_{\text{ch}}}{(P_{\text{ASE}}^{1 \text{ span}} + P_{\text{NLI}}^{1 \text{ span}}) N_s} \quad (50)$$

where $P_{\text{ASE}}^{1 \text{ span}}$ is the ASE noise due to a single amplifier, which we approximate as:

$$P_{\text{ASE}}^{1 \text{ span}} = h\nu F (\Lambda - 1) R_s \approx h\nu F \Lambda R_s \quad (51)$$

where the quantity Λ is the optical amplifier gain. We then define:

$$\eta^{1 \text{ span}} = P_{\text{NLI}}^{1 \text{ span}} / P_{\text{ch}}^3 \quad (52)$$

It can easily be shown, based on the GN/IGN-model, that $\eta^{1 \text{ span}}$ is independent of P_{ch} , through the same reasoning used to prove the same property for the parameter η in Sect. IV-A. We can then write:

$$\text{SNR}_{\text{NL}} = \frac{P_{\text{ch}}}{(P_{\text{ASE}}^{1 \text{ span}} + \eta^{1 \text{ span}} \cdot P_{\text{ch}}^3) N_s} \quad (53)$$

where the overall dependence on P_{ch} has been made explicit.

We are interested in the system reach. Therefore we bring out N_s and we impose that SNR_{NL} be equal to the chosen system target value SNR_{T} . The resulting reach is:

$$N_s = \frac{P_{\text{ch}}}{(P_{\text{ASE}}^{1 \text{ span}} + \eta^{1 \text{ span}} \cdot P_{\text{ch}}^3) \cdot \text{SNR}_{\text{T}}} \quad (54)$$

With simple calculus, the optimum launch power $P_{\text{ch}}^{\text{opt}}$, i.e., the one maximizing N_s , is found to be:

$$P_{\text{ch}}^{\text{opt}} = \sqrt[3]{P_{\text{ASE}}^{1 \text{ span}} / (2 \eta^{1 \text{ span}})} \quad (55)$$

Substituting this value of launch power back into Eq. (54), the MSR is finally found:

$$N_s^{\text{max}} = \frac{1}{3 \text{SNR}_{\text{T}}} \sqrt[3]{\frac{4}{(P_{\text{ASE}}^{1 \text{ span}})^2 \cdot \eta^{1 \text{ span}}}} \quad (56)$$

The NLI parameter $\eta^{1\text{ span}} = G_{\text{NLI}}^{1\text{ span}} \cdot (R_s/P_{\text{ch}}^3)$ can be calculated using the GNRF. However, in order to obtain closed-form formulas, we use the GNRF approximation Eq. (40), with the substitutions $B_{\text{ch}} \approx R_s$ and $G_{\text{WDM}} \approx P_{\text{ch}}/R_s$:

$$\eta^{1\text{ span}} \approx \frac{8}{27} \frac{\gamma^2 L_{\text{eff}}^2}{\pi |\beta_2| R_s^2 L_{\text{eff},a}} \operatorname{asinh} \left(\frac{\pi^2}{2} |\beta_2| L_{\text{eff},a} R_s^2 N_{\text{ch}}^2 \frac{R_s}{\Delta f_{\text{ch}}} \right) \quad (57)$$

Eqs. (51), (56)-(57), already provide a closed-form equation set to estimate the MSR. However, individual parameter dependencies are still rather involved. Further manipulations are needed to bring out such dependencies.

One hurdle towards this goal is the presence of the asinh function in Eq. (57). On the other hand, $\operatorname{asinh}(x) \approx \log_e(2x)$ so it could be claimed that the variations of the asinh factor vs. its argument are typically very weak. Using this and other arguments, we finally obtain a drastic approximation to Eq. (57), which reads:

$$\eta^{1\text{ span}} \approx C \frac{R_s}{\Delta f_{\text{ch}}} \frac{\alpha_{\text{dB}} \gamma^2 L_{\text{eff}}^2}{|D| R_s^2} \quad (58)$$

where C is a constant. Some of the parameters were replaced by those typically used in the industry. Specifically, α_{dB} , fiber power loss in [dB/km], and D , fiber dispersion in [ps/(nm km)], replaced α and β_2 , respectively.

The validation of this expression is dealt with in the next section. For now, we assume that it is accurate enough for our purposes.

Placing Eq. (58) into Eqs. (55)-(56), it is then possible to derive simple variational laws for $N_{s,\text{dB}}^{\text{max}}$ and $P_{\text{ch,dB}}^{\text{opt}}$ as a function of the main system parameters. Using convenient dB units, they are:

$$\begin{aligned} \Delta P_{\text{ch,dB}}^{\text{opt}} &= 10 \log_{10} \left(\frac{P_{\text{ch}}^{\text{opt}}}{P_{\text{ch,ref}}^{\text{opt}}} \right) = \\ &\frac{1}{3} (\Delta \alpha_{\text{dB}} + \delta A_{s,\text{dB}}) + \frac{1}{3} (\Delta D_{\text{dB}} - 2\Delta \gamma_{\text{dB}}) + \\ &+ \frac{1}{3} \delta F_{\text{dB}} + \frac{1}{3} (\Delta K_{s,\text{dB}} + 3\Delta R_{s,\text{dB}}) \end{aligned} \quad (59)$$

$$\begin{aligned} \Delta N_{s,\text{dB}}^{\text{max}} &= 10 \log_{10} \left(\frac{N_{s,\text{dB}}^{\text{max}}}{N_{s,\text{ref}}^{\text{max}}} \right) = \\ &\frac{1}{3} (\Delta \alpha_{\text{dB}} - 2\delta A_{s,\text{dB}}) + \frac{1}{3} (\Delta D_{\text{dB}} - 2\Delta \gamma_{\text{dB}}) + \\ &- \frac{1}{3} (3\delta \text{SNR}_{\text{T,dB}} + 2\delta F_{\text{dB}}) + \frac{1}{3} \Delta K_{s,\text{dB}} \end{aligned} \quad (60)$$

where the parameter variations with respect to a reference scenario (subscript ‘ref’) are:

- $\Delta \alpha_{\text{dB}} = 10 \cdot \log_{10} \left(\frac{\alpha_{\text{dB}}}{\alpha_{\text{dB,ref}}} \right)$;
- $\delta A_{s,\text{dB}} = A_{s,\text{dB}} - A_{s,\text{dB,ref}}$;
- $\Delta D_{\text{dB}} = 10 \cdot \log_{10} \left(\frac{D}{D_{\text{ref}}} \right)$;
- $\Delta \gamma_{\text{dB}} = 10 \cdot \log_{10} \left(\frac{\gamma}{\gamma_{\text{ref}}} \right)$;
- $\delta \text{SNR}_{\text{T,dB}} = \text{SNR}_{\text{T,dB}} - \text{SNR}_{\text{T,dB,ref}}$;
- $\delta F_{\text{dB}} = F_{\text{dB}} - F_{\text{dB,ref}}$;
- $\Delta R_{s,\text{dB}} = 10 \cdot \log_{10} \left(\frac{R_s}{R_{s,\text{ref}}} \right)$;
- $\Delta K_{s,\text{dB}} = 10 \cdot \log_{10} \left(\frac{K_s}{K_{s,\text{ref}}} \right)$.

We used two new parameters, namely: $K_s = \Delta f_{\text{ch}}/R_s$ and A_s . The former is the channel spacing relative to the symbol rate. The latter accounts for total span loss, due to both fiber and other components. Note that the each amplifier in the link,

SYSTEM	R_s [GBaud] $K_s = \Delta f_{\text{ch}}/R_s$	FIBER	MSR N_s^{max}	
reference simulation 200G PM-16QAM	$R_s = 32$ $K_s = 1.05$	SMF	15	
[58] 100G PM-QPSK	$R_s = 30$ $K_s = 1.1$	NZDSF SMF PSCF	8 20 32	Eq. (60) 7 20 31
[59] 100G PM-16QAM	$R_s = 15.625$ $K_s = 1.024$	NZDSF SMF PSCF80 PSCF110 PSCF130 PSCF150	12 38 44 58 62 70	Eq. (60) 11 39 45 57 63 70

TABLE II
COMPARISON BETWEEN MAXIMUM SYSTEM REACH FROM EXPERIMENTS AND AS PREDICTED BY EQ. (60)

due to the transparency assumption, exactly delivers a gain such that $\Lambda = A_s$.

Note also that the value of the constant C in Eq. (58) appears nowhere in either Eqs. (59) or (60). This is because, when variations are addressed, it cancels out. This is a very favorable aspect, as it means that the variational dependencies established by Eqs. (59) and (60) are in fact formally *independent* of the starting reference system scenario.

From Eqs. (59) and (60), the following two general properties can then be derived:

- $P_{\text{ch}}^{\text{opt}}$ does not depend on SNR_{T} : this means that the optimum launch power is independent of either modulation format, FEC gain, or even transponder penalties;
- the MSR is independent of the symbol rate, given the target performance SNR_{T} and the relative channel spacing K_s .

Eqs. (59)-(60) provide a dB-by-dB dependence of $P_{\text{ch}}^{\text{opt}}$ and MSR on all the listed parameters. It is interesting to see, for instance, that a 3-dB increase in amplifier noise figure causes a 1 dB increase in $P_{\text{ch}}^{\text{opt}}$, while at the same time the MSR goes down by 2 dB. The role of dispersion, not quite recognized until recently, is also clearly visible, in the sense that a larger D improves the MSR, albeit with a 1/3 attenuation factor, dB-over-dB.

A. Comparison with experiments

A possible method for the validation of Eqs. (59) and (60), and indirectly of Eq. (58), consists in establishing a reference system scenario and then apply changes to it. If the effects of the changes are correctly predicted, then this indicates that the variational laws are reliable.

We chose to do this by first establishing a reference scenario through simulations. Then we computed the variations to match the system parameters of the experiments [58]-[59]. We then predicted MSRs by adding the MSR of the reference scenario to the MSR variation given by Eq. (60). Finally, we compared the predicted MSR with those actually found in the experiments.

The reference scenario was as follows: UT, 9 channels, 200G PM-16QAM transmission, $R_{s,\text{ref}} = 32$ GBaud, $K_{s,\text{ref}} = 1.05$, SMF with $L_{\text{span},\text{ref}} = 80$ km, $\alpha_{\text{dB},\text{ref}} = 0.22$ dB/km, $A_{s,\text{dB},\text{ref}} = 17.6$ dB, $D_{\text{ref}} = 16.7$ ps/(nm km), $\gamma_{\text{ref}} = 1.3$ 1/W/km, $F_{\text{dB},\text{ref}} = 5$ dB. The target BER was 10^{-3} corresponding to $\text{SNR}_{\text{T,dB},\text{ref}} = 16.85$ dB. The simulation resulted in $N_{s,\text{ref}}^{\text{max}} = 15$.

Then, we estimated the maximum reach of each experiment as:

$$N_s^{\text{max}} = N_{s,\text{ref}}^{\text{max}} \cdot 10^{\frac{\Delta N_{s,\text{dB}}^{\text{max}}}{10}} \quad (61)$$

where $\Delta N_{s,\text{dB}}^{\text{max}}$ was calculated using Eq. (60).

The first considered experiment [58] was a 10-channel NyWDM 100G PM-QPSK setup ($R_s = 30$ GBaud, $K_s = 1.1$) comparing max reach of 3 fibers at $\text{BER} = 10^{-3}$ ($\text{SNR}_{\text{T,dB}} = 12.7$ dB). The second one [59] was a 22-channel NyWDM 100G PM-16QAM setup ($R_s = 15.625$ GBaud, $K_s = 1.024$) that investigated the max reach over 7 different fiber types at $\text{BER} = 10^{-2}$ ($\text{SNR}_{\text{T,dB}} = 17.3$ dB). Regarding the second experiment, we did not consider the results of propagation over DCF used as transmission fiber, as this scenario is clearly outside of the scope of practical systems. For the other six fibers, besides the parameters listed in [59], we included the following measured insertion extra losses: 2 dB (NZDSF), 0 dB (SSMF), 0.3 dB (PSCF80), 0.4 dB (PSCF110), 0.6 dB (PSCF130 and PSCF150) which were not explicitly reported in [59].

As it can be observed in Tab. II, the prediction accuracy with respect to the experimental results is always within 1 span. It confirms the reliability of the proposed formulas, even when applied to different modulation formats and rates, for a wide range of fiber types. Certainly, more validation is necessary, but these preliminary results indicate that, despite the drastic approximations used, the found ‘design rules’ do provide useful coarse variational information.

VIII. ASSESSING OPTICAL SYSTEM THROUGHPUT USING THE GN-MODEL

An important research topic in the field of optical communications is that of the determination of the ‘capacity’ of the optical channel. A problem that is immediately encountered when dealing with this topic is one of definitions and assumptions³. Rather than discussing here the complex aspects of how to suitably define capacity for the optical channel and how to properly estimate it, we refer the reader to [69] (esp. Sect. III and XII), where these aspects were quite extensively dealt with.

Our goal here is however different from capacity estimation, although related to it. Rather than estimating capacity, which is the ‘ultimate’ throughput which can be achieved under certain optimal conditions [69], we are interested in the *actual* throughput of current optical systems, under practical and realistic conditions.

³Depending on them, rather different capacity results can be arrived at. For instance, in [69] capacity curves always present a well-defined maximum vs. launch power, whereas in [70] it is argued that capacity may be non-decreasing vs. increasing launch power.

As a result, differently from [69], we will refrain from assuming that the system makes use of NLI compensation by means of single-channel backward-propagation (BP), a technique which, though certainly effective, is still regarded as beyond the computational power of current DSPs. Only in one case we will assume single-channel NLI compensation (namely, for a Gaussian constellation at the Nyquist limit) to show that our results match those of [69].

In all other cases, we investigate practical Tx formats without BP and show some realistic OCT results and trade-offs which are directly relevant to modern high-capacity long-haul systems.

Most important, our throughput estimates will be based on the use the GN-model to assess the impact of NLI. Besides showing specific results, we are outlining a procedure for obtaining throughput results, that the readers can easily adapt to their systems of interest.

A. Approach

As pointed out in [69], a *lower-bound* to the capacity of an optical channel can be obtained by estimating the mutual information $I(X, Y)$ between the Tx-side input alphabet X and the Rx-side output alphabet Y , assuming a *memoryless* model for the channel. The reasons and proof why this is a lower bound can be found in [69], Sect. III-F.

All the results shown in [69] were based on a memoryless model for the channel. To make them reasonably accurate, in [69] single-channel backward propagation (BP) was applied to the channel under test. This roughly amounts to eliminating the channel memory due to linear effects and to single-channel NLI. However, all of the disturbance due to XCI and MCI retains its memory, making the results of [69] ‘lower bound estimates of the actual capacity’, as explicitly stated in Sect. III-F there.

On the other hand, the same results, while being capacity lower-bounds, provide the *actual* throughput of a channel which operates according to the stated assumption. In other words, they provide the actual optical channel throughput (OCT) of systems using single-channel BP.

If instead of BP, only linear-effect compensation is assumed for the channel under test, then the memoryless estimate of $I(X, Y)$ provides again a lower bound to the channel capacity, according to the proof shown in Sect. III-F of [69]. This bound is of course looser than the one found assuming single-channel BP. However, it provides the *actual* throughput of a channel which operates according to just linear effect compensation.

This latter circumstance is important because it shows that a study directed towards assessing the actual OCT of linear-compensation-only systems can in fact be based on a memoryless estimate of $I(X, Y)$. This is indeed the actual goal of this section. The fact that such estimate also constitutes a (loose) lower bound to capacity is, in the context of this study, incidental, and not the essential goal.

In the following, we will make the LWN approximation for NLI. As discussed in Sect. IV-B, this approximation does cause some error, although its impact on the center channel of a comb is negligible if full spectral loading (C band) is

assumed together with tight channel spacing. We will also assume that all channels have the same NLI as the center channel. This is well verified over about half of the comb, whereas the outer edge channels in the WDM comb experience somewhat less NLI (see Sect. IV-B). In principle, it would be possible to address this aspect too by, for instance, finding the optimum non-uniform per-channel launch power in the comb. However, we decided to neglect this aspect, while pointing out that this leads to slightly under-estimating OCT.

The combination of the memoryless and LWN assumptions make the channel that we consider coincide with the well-known memoryless AWGN channel. To find its throughput we can then use the analytical AWGN capacity formulas, written as a function of a suitable SNR. In our case such SNR is related to SNR_{NL} of Eq. (22) and we will use the GN-model results to estimate it. In particular, the values of P_{NLI} can be obtained either using analytical formulas, when available, or by numerically integrating the general expression of G_{NLI} , reported in Eq. (1).

In a few special cases, the resulting OCT has a closed-form expression. One example is shown in Sect. VIII-B, for an optical channel with continuous input and output alphabets and ideal distributed amplification. Note that we address this highly idealized case only to perform a direct comparison with the corresponding results found in [69] and thus validate the overall approach.

Sect. VIII-C reports on the results of the OCT evaluation in a more realistic case of a discrete-input channel using standard PM constellations (ranging from PM-QPSK to PM-64QAM), in different system scenarios employing either EDFA or hybrid Raman/EDFA amplification.

B. Continuous-input, continuous-output optical channels with ideal distributed amplification

Keeping in mind the assumptions of Sect. VIII-A, resorting to Shannon's formula [68] for the unconstrained additive white-Gaussian-noise (AWGN) channel capacity $C = \log_2(1 + \text{SNR})$ [bit/s/Hz], it is possible to derive a similar formula for the single-polarization (SP) and the polarization-multiplexed (PM) memoryless channel OCT:

$$\text{OCT} = p \frac{R_s}{\Delta f_{\text{ch}}} \log_2 \left(1 + \frac{2}{p} \text{SNR}_{\text{NL}} \right) \quad [\text{bit/symbol}] \quad (62)$$

where $p=1$ for a single-polarization signal and $p=2$ for a polarization-multiplexed signal. This formula assumes that the input constellation has an ideal Gaussian distribution.

In the case of distributed amplification (DA), the ASE noise power (sum over both polarizations) can be expressed as:

$$P_{\text{ASE,DA}} = 4\alpha L_{\text{tot}} h\nu K_T R_s \quad (63)$$

where h is Planck's constant, ν is the center frequency of the WDM comb and $K_T \geq 1$ is a constant which is approximately equal to 1.13 for realistic Raman amplification [69].

Assuming to work at the Nyquist limit, i.e. the channels of the WDM comb have a rectangular spectrum, with bandwidth and frequency spacing equal to the symbol rate, using Eq. (37)

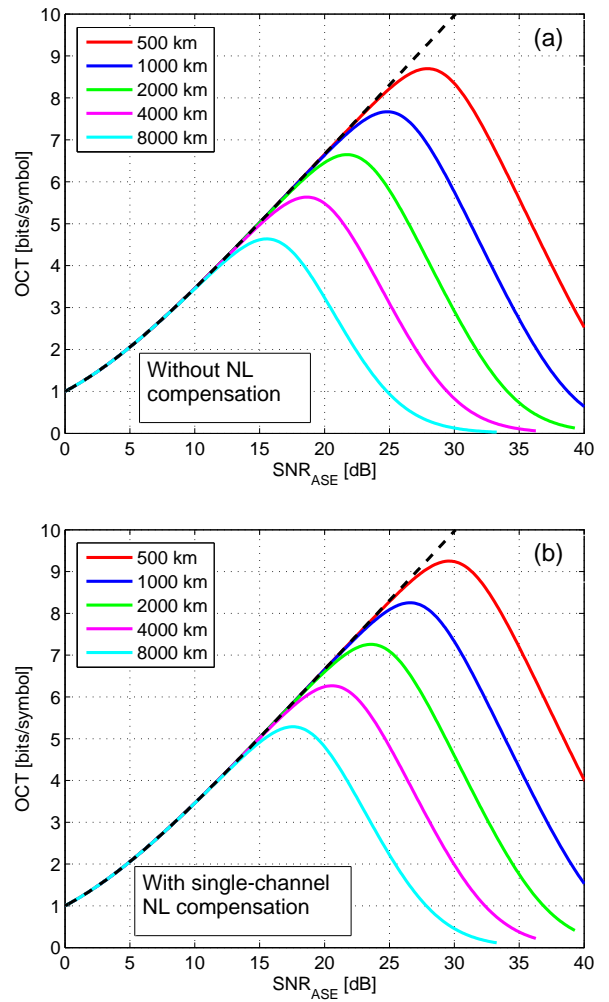


Fig. 10. Optical channel throughput (OCT) versus signal-to-noise ratio due to ASE only, for 500 km (red), 1000 km (blue), 2000 km (green), 4000 km (purple), and 8000 km (cyan). The black dashed line is the AWGN Shannon limit. (a) Without NL compensation. (b) With single-channel NL compensation.

P_{NLI} can be written analytically as:

$$P_{\text{NLI}} \approx K_p \gamma^2 L_{\text{tot}} P_{\text{ch}}^3 \frac{\text{asinh} \left(\frac{1}{3} \pi^2 |\beta_2| L_{\text{tot}} B_{\text{WDM}}^2 \right)}{\pi |\beta_2| R_s^3} R_s \quad (64)$$

where $K_p = 2$ for single polarization and $K_p = 16/27$ for polarization multiplexing.

It is thus possible to write the OCT of optical WDM systems working at the Nyquist limit and using ideal distributed amplification in a closed-form, as shown in Eq.(65).

As an example, in Fig. 10(a), we use Eq. (65) to plot the OCT vs. the SNR due to ASE noise only ($\text{SNR}_{\text{ASE}} = P_{\text{ch}}/P_{\text{ASE}}$) in a single-polarization optical link with ideal distributed amplification, for different link lengths. The number of WDM channels is equal to 5, with symbol rate $R_s = 100$ GBaud, and the fiber is standard single-mode (SMF) with same parameters as in [69]: $\gamma = 1.27$ 1/W/km, $\alpha = 0.22$ dB/km, $\beta_2 = -21.7$ ps²/km. The reason for choosing these specific system parameters is that they are the ones used in [69] (see Sect. XII, Tables I-III) and we would like to compare our results with those found there. For the same reason, the

$$\text{OCT}_{\text{DA}} = p \frac{R_s}{\Delta f_{\text{ch}}} \log_2 \left(1 + \frac{2}{p} \frac{P_{\text{ch}}}{\left(4\alpha L_{\text{tot}} h\nu K_T + K_p \gamma^2 L_{\text{tot}} P_{\text{ch}}^3 \frac{\text{asinh}\left(\frac{1}{3}\pi^2|\beta_2|L_{\text{tot}}B_{\text{WDM}}^2\right)}{\pi|\beta_2|R_s^3} \right)} \right) R_s \quad (65)$$

distributed amplification noise parameter K_T is set here to 1, rather than 1.13.

Fig. 10(a) appears to be similar to Fig. 35 in [69]. Our values are slightly less than those in [69], due to the fact that [69] used (single-channel) BP non-linear compensation (NLC) in the receiver simulation.

In order to make our results fully comparable to those in [69], we analytically took single-channel NLC into account by evaluating the amount of NLI generated by the single-channel alone ($P_{\text{NLI},1\text{ch}} = P_{\text{NLI}}|_{N_{\text{ch}}=1}$), and subtracting that value from P_{NLI} :

$$P_{\text{NLI},\text{res}} = P_{\text{NLI}} - P_{\text{NLI},1\text{ch}} \quad (66)$$

where $P_{\text{NLI},\text{res}}$ is the residual value of NLI which impacts the system after NLC. Further details on NLC can be found in Sect. IX.

The obtained results are reported in Fig. 10(b), which shows a good agreement with Fig. 35 in [69]. The slightly better performance observed in Fig. 10(b) is likely due to the fact that our analysis assumes an ideal Gaussian constellation, while the simulations in [69] were performed using the ring constellation approximation. The good correspondence between our analytical calculations and the simulative results of [69] indicates that our GN-model based approach returns rather reliable OCT results.

C. Discrete-input, continuous-output optical channels

The derivation of the OCT formula in Sect. VIII-B is based on the hypothesis of an ideal continuous input alphabet with Gaussian distribution. However, real systems are based on the use of a discrete input alphabet, usually composed of multi-level QAM constellations. In this section, we will assess the OCT of a polarization-multiplexed uncompensated optical system with coherent detection, using PM-QAM modulation formats with cardinality equal to 4, 8, 16, 32 and 64. We assume a continuous-output alphabet, which corresponds to using soft-decision forward-error correction (FEC) schemes. The DSP is assumed to compensate for linear effects only.

In order to obtain throughput estimates we can then adapt to our case the standard formulas of capacity over AWGN [56], [68]. Assuming that all symbols have the same a priori probability, the OCT can be evaluated as:

$$\text{OCT} = 2 \frac{R_s}{\Delta f} \frac{1}{M} \sum_{a \in X} \int p_{Y|X}(y|a) \log_2 \frac{p_{Y|X}(y|a)}{p_Y(y)} \quad (67)$$

where M is the number of constellation points, $X = \{x_1, \dots, x_M\}$ is the set of possible transmitted symbols, $y = y_r + j y_i$ is the soft value at the output of the channel, $p_{Y|X}(y|a)$ is the probability density function of the random

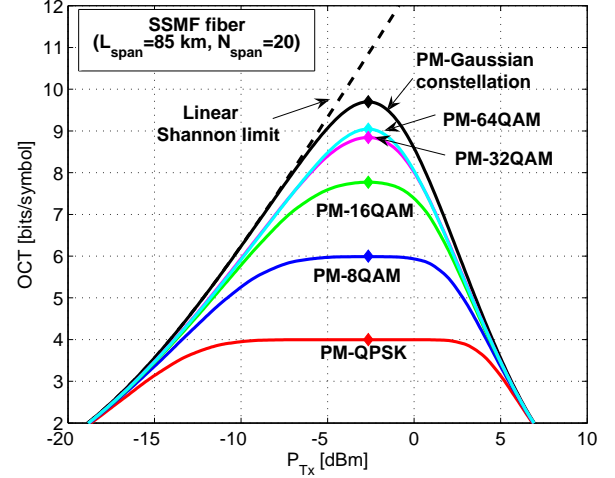


Fig. 11. Optical channel throughput (OCT) versus transmitted power per channel P_{ch} (called P_{Tx} in figure) over 20 spans of SMF ($L_s=85$ km), assuming different modulation formats and DSP compensation of linear effects only. The black dashed line is the conventional Shannon limit in additive white-Gaussian noise, called ‘linear’.

variable y , $p_Y(y)$, conditioned to the transmission of the symbol $a = a_r + j a_i$.

Assuming transmission over a memoryless AWGN channel and using standard probability theory results [56], it is possible to evaluate analytically all probabilities in Eq. (67) in terms of SNR at the receiver:

$$p_{Y|X}(y|a) = \frac{1}{\pi\sigma_N^2} \exp\left\{-\frac{(y_r - a_r)^2 + (y_i - a_i)^2}{\sigma_N^2}\right\} \quad (68)$$

$$p_Y(y) = \frac{1}{M} \sum_a p_{Y|X}(y|a)$$

where σ_N^2 is the noise variance at the Rx decision stage, which is inversely proportional to the SNR value:

$$\text{SNR} = \frac{P_s}{\sigma_N^2} \quad (69)$$

with P_s average power per symbol of the Rx constellation.

Equivalently, the OCT can also be evaluated as:

$$\text{OCT} = 2 \frac{R_s}{\Delta f} (H(Y) - \ln(\pi\sigma_N^2)) \quad (70)$$

with:

$$H(Y) = - \int p_Y(y) \log_2(p_Y(y)) \quad (71)$$

As an example, in Fig. 11 the values of OCT obtained for PM-QPSK, PM-8QAM, PM-16QAM, PM-32QAM and PM-64QAM with soft decision and EDFA amplification are shown over 20 spans of SMF fiber ($L_{\text{span}}=85$ km). We assumed C-band transmission ($B_{\text{WDM}}=5$ THz) at the Nyquist limit.

TABLE III

RAW (PRE-FEC) BER VALUES CORRESPONDING TO THE MAXIMUM OPTICAL CHANNEL THROUGHPUT POINTS SHOWN AS DIAMOND MARKERS IN FIG. 11

PM-QPSK	$6.6 \cdot 10^{-8}$
PM-8QAM	$3.7 \cdot 10^{-4}$
PM-16QAM	$6.9 \cdot 10^{-3}$
PM-32QAM	$3.2 \cdot 10^{-2}$
PM-64QAM	$7.3 \cdot 10^{-2}$

Note that at the Nyquist limit OCT coincides with the system ‘spectral efficiency’ (SE), in bit/(s·Hz). This circumstance was also pointed out in [69], where Nyquist-limit plots were quoted as ‘spectral efficiency’ ([69], Figs. 32-38).

The plateau of 4 bit/symbol and 6 bit/symbol reached by PM-QPSK and PM-8QAM, respectively, means that, at this link length, the OCT is limited by the cardinality of the constellation rather than by signal degradation. This means that the ‘asymptotic effect’, caused by the finite number of constellation symbols, occurs largely before the limitation due to non linear effects. PM-16QAM almost reaches its 8 bit/symbol theoretical maximum, while both PM-32QAM and PM-64QAM are significantly limited and fall well short of their ideal 10 and 12 bit/s/Hz. The PM-Gaussian constellation is theoretically optimum and therefore it outperforms all other formats. For all formats, the optimum launch power per channel, i.e. the value of P_{ch} maximizing the OCT, is equal to -2.65 dBm.

Note that the OCT maximum is reached at very different BER values among formats. It is in fact their high pre-FEC BER values that make PM-32/64QAM OCT substantially lower than ideal. The values of pre-FEC BER corresponding to the maximum OCT points (diamond markers in Fig. 11) are shown in Table III. Note also that the ratio between the lost OCT and the maximum OCT of a certain format corresponds to the minimum required ideal FEC overhead necessary to obtain an arbitrarily low BER [56]. Practical FECs of course need higher overheads, although state-of-the-art FECs come rather close to the minimum required overhead: for state-of-the-art soft FEC codes the estimated coding gain penalty vs. the ideal maximum gain is around 1.5 dB.

D. OCT vs. distance analysis

Thanks to the OCT formulas derived with the GN-model, we can analyze the relationship between OCT and total link length for realistic formats and in arbitrary transmission scenarios. In this section, we exemplify this possibility by analyzing PM-QAM formats in three different link scenarios:

- **Link 1:** Terrestrial link over SMF with EDFA-only amplification ($F=5$ dB) and 85-km span length;
- **Link 2:** Terrestrial link over SMF with hybrid EDFA/Raman amplification (equivalent $F=0$ dB) and 120-km span length;
- **Link 3:** Submarine link over PSCF with EDFA-only amplification ($F=5$ dB) and 50-km span length.

The parameters of the fibers are shown in Table I. The WDM signal is assumed to occupy the entire C-band ($B_{WDM}=5$ THz)

at the Nyquist limit (i.e. with $\Delta f_{ch} = R_s$). In order to analyze a realistic scenario, we assumed to operate with a conservative 3-dB margin with respect to the ideal BER-vs.-SNR performance and with a realistic soft FEC 1.5-dB penalty with respect to ideal soft-FEC performance.

The dependence of the OCT on total link length is plotted in Fig. 12 for PM-QAM modulation formats with cardinality ranging from 4 to 64. The curves obtained with an ideal Gaussian constellation are also shown. The results of Figs. 12 clearly highlight the trade-off between distance and OCT, in relation to the different modulation formats: increasing the cardinality of the constellation, a higher OCT can be achieved, but typically over a shorter transmission distance and/or at a higher required FEC overhead. Note that the performance achievable over Link 1 and Link 2 is very similar, due to the fact that the noise figure reduction due to Raman amplification (from 5 to 0 dB) almost completely compensates the higher loss due to longer span length ($\simeq 6$ dB).

State-of-the-art soft FEC with 20% overhead can now operate at pre-FEC BER of $2.7 \cdot 10^{-2}$ [71]: so, for all modulation formats, the points corresponding to $BER=2.7 \cdot 10^{-2}$ are marked in the figures. The section of the OCT lines to the left of the dots is therefore the ‘practicable’ section, whereas moving to the right will be possible only if better FECs become available.

Considering the currently possible systems, in a terrestrial link with EDFA only amplification (Link 1), PM-QPSK is the best choice for ultra-long-haul transmissions beyond 5,000 km, while PM-8QAM can be used to achieve an OCT around 5-5.5 bit/symbol (or SE in bit/(s·Hz)) in 3,000 km links. PM-16QAM allows to reach 2,000 km with an $OCT \simeq 6.5$ bit/symbol. The reach of higher-order modulation formats, like PM-32QAM or PM-64-QAM, is very limited in this kind of systems, but can be significantly increased by using new generation fibers and shorter span length, like in the analyzed submarine-like system (Link 3), where they reach 2,400 km and 1,800 km, respectively. The plot also shows that PM-16QAM could reach ultra-long-haul distances (beyond 6,000 km with 20% hard-FEC overhead) over submarine-like links. Note that this reach can be further increased by using better-performing fibers, higher-performance FEC and NL compensation techniques at the Rx, as done in [76], where 10,000 km could be achieved at a SE of 6 bit/(s·Hz).

IX. COMBATING NON-LINEARITY

In this section we present another significant example of the application of the GN-model, in which the GN-model provides clear answers, with high potential impact.

In coherent systems, linear transmission impairments can be almost totally compensated for using DSP, with reasonable computational complexity [72]. Recently, substantial efforts have been aimed at investigating the possibility of using DSP to mitigate non-linear effects too. Several non-linear compensation (NLC) algorithms have been proposed, among which: digital back-propagation (DBP) [73]-[75], Volterra series techniques [78] and MLSE-based techniques [79].

All of these algorithms appear to have one major fundamental limitation. They can only mitigate the NLI that is strictly

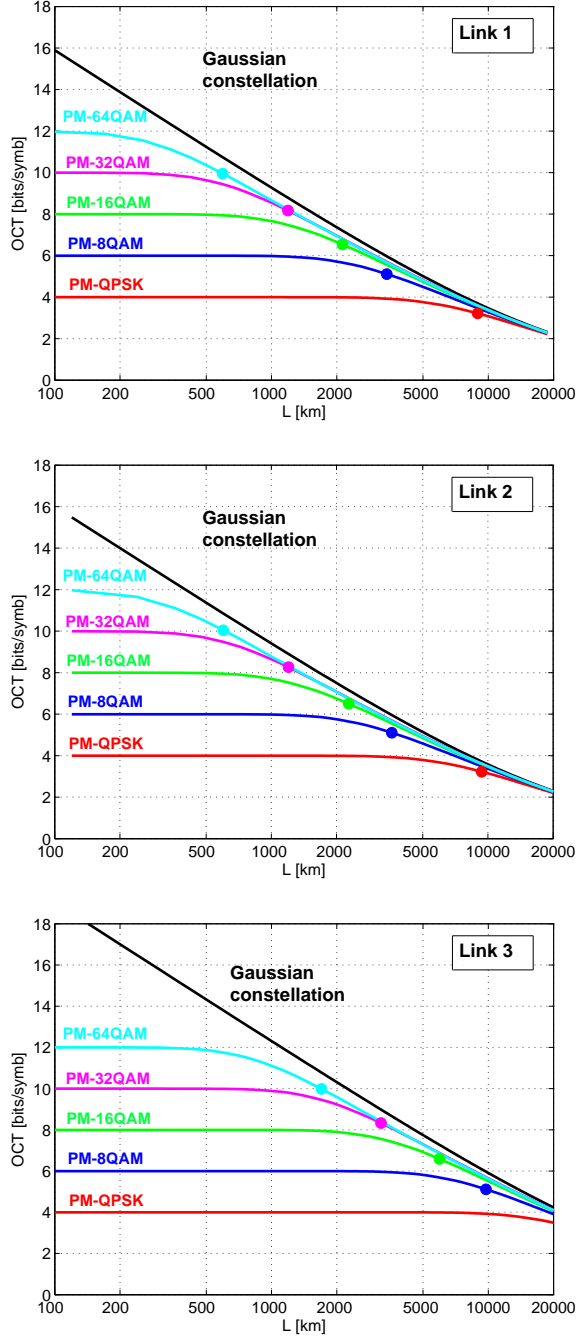


Fig. 12. Optical channel throughput (OCT) versus total link length in three different transmission scenarios described in the text. $B_{\text{WDM}}=5$ THz, $\Delta f_{\text{ch}} = R_s$. Assumptions: 3-dB SNR penalty from quantum limit and 1.5-dB penalty of soft FEC with respect to infinite-length codes ideal performance. Dots correspond to a pre-FEC $\text{BER}=2.7 \cdot 10^{-2}$.

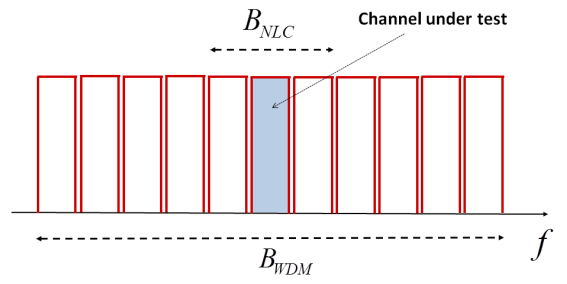


Fig. 13. WDM comb: $B_{\text{WDM}} = N_{\text{ch}} \cdot \Delta f_{\text{ch}}$ is the total occupied bandwidth, while B_{NLC} is the bandwidth over which non-linear compensation is applied.

generated within the spectral window that the algorithm has access to. Specifically, if the algorithm operates within the DSP of a single Rx, whose bandwidth encompasses a single channel, then only the NLI produced by the channel onto itself (namely, SCI) can be mitigated. No effect can be expected on XCI and MCI, that is on NLI produced cooperatively with the other WDM channels. This circumstance was experimentally recognized early on [74] and has been confirmed by later investigation.

Ideally, this problem can be dealt with by providing the DSP with more spectral visibility, or ‘optical compensation bandwidth’ B_{NLC} . This can be done by either increasing the bandwidth of each single Rx or by exchanging the soft samples of the received signal among some or all the WDM Rx’s. Unfortunately, non-linearity mitigation techniques are extremely computationally intensive, already at the single-channel level. Extending the bandwidth they operate on, strongly exacerbates this problem. So, a careful cost/benefit assessment is needed. Such cost/benefit analysis can be carried out using the GN-model, as is shown in the following.

A. Limits of DSP Non-Linearity Compensation

We assume that the NLC algorithm has the knowledge of the signal over an optical compensation bandwidth B_{NLC} (see Fig. 13). In order to derive an *upper bound* to the possible performance gain, we make the ideal assumption that the NLC algorithm is able to *completely* cancel out the NLI generated by all WDM signal components inside the bandwidth B_{NLC} .

We investigated a set of systems with the following parameters:

- transparent and homogenous link with identical equi-spaced channels
- symbol rate R_s : 32 GBaud
- frequency spacing Δf_{ch} : 32, 40 and 50 GHz
- large effective area PSCF (see Table I) with $L_s=85$ km.

Note that the transmission format is not indicated because results are independent of it. Transmission spectra are assumed to be perfectly rectangular. In any case, the roll-off parameter has very little impact on the results. We assume that the total bandwidth B_{WDM} occupied by the WDM comb is the whole C-band (5 THz) and that the B_{NLC} ranges from a minimum value equal to R_s (corresponding to a single-channel) to a maximum of B_{WDM} .

We analytically took NLC into account by evaluating the amount of NLI generated within the compensation bandwidth

B_{NLC} , that we call $P_{\text{NLI},B_{\text{NLC}}}$, and then subtracting that value from the total P_{NLI} . The residual value of NLI impacting the system is then:

$$P_{\text{NLI, res}} = P_{\text{NLI}} - P_{\text{NLI},B_{\text{NLC}}} \quad (72)$$

All calculations were performed assuming coherent NLI accumulation, i.e., using the GNRF of Eq. (2).

The results on the effectiveness of NLC are shown in Fig. 14 in terms of $\Delta P_{\text{NLI,dB}}$, defined as the ratio in dB between the total NLI generated during propagation and the residual NLI after compensation:

$$\Delta P_{\text{NLI,dB}} = 10 \log_{10} \left(\frac{P_{\text{NLI}}}{P_{\text{NLI, res}}} \right) \quad (73)$$

This ratio is power-independent and therefore the launch power is not a relevant system parameter in the calculations. $P_{\text{NLI,dB}}$ can be considered as the ‘NLC gain’, in dB, that can be obtained, for each given value of B_{NLC} .

Fig. 14 shows that the NLC gain increases with the number of spans: as an example, single-channel NLC at 32-GHz channel spacing achieves 0.8 dB NLC gain after a single span but 2.2 dB after 40 spans. This is due to the greater coherency in the accumulation of SCI than XCI or MCI. Further increasing the number of spans (not shown) does not however result in anymore significant increase in NLC gain.

For low values of B_{NLC} , the NLC gain is higher when the channel spacing is larger, since the relative strength of SCI increases as the spacing goes up. However, when B_{NLC} increases, the NLC gain tends to become the same at all considered values of Δf_{ch} . Finally, when $B_{\text{NLC}} = B_{\text{WDM}}$, full ‘visibility’ of the optical spectrum is achieved by the NLC algorithm and, ideally, all nonlinearity is compensated for. As a result, the NLC gain ideally goes to infinity.

Not shown for brevity, we redid the analytical evaluation of NLC gain for the same system, with the same span length, but over SMF and NZDSF. The results are qualitatively similar to those for the PSCF. Quantitatively, they are somewhat worse, because an even higher B_{NLC} is needed to obtain the same NLC gain. The reason is that NLC gain decreases slightly as either dispersion decreases or loss increases, which makes SMF and NZDSF less favorable fibers for NLC than PSCF.

B. Maximum reach gain due to NLC

The NLC gain of Fig. 14 does not directly translate into an MSR gain. Similarly to what was shown in Sect. IV-A, it can be predicted that:

$$\Delta N_{s,\text{dB}}^{\text{max}} \approx \frac{1}{3} \Delta P_{\text{NLI,dB}} \quad (74)$$

where $\Delta N_{s,\text{dB}}^{\text{max}}$ is the ratio, in dB, of the MSR with and without NLC. According to Eq. (74), a 3-dB compensation of NLI would only translate into about a 1-dB gain in MSR (26%).

Since this is a key aspect, we decided to analyze the MSR without resorting to approximate formulas such as Eq. (74). We performed a full system MSR evaluation, assuming PM-16QAM, PSCF with $L_s=85$ km, $\Delta f_{\text{ch}}=32, 40, 50$ GHz, target $\text{BER}=2 \cdot 10^{-3}$, $B_{\text{WDM}}=5$ THz, EDFA noise figure 5 dB. The

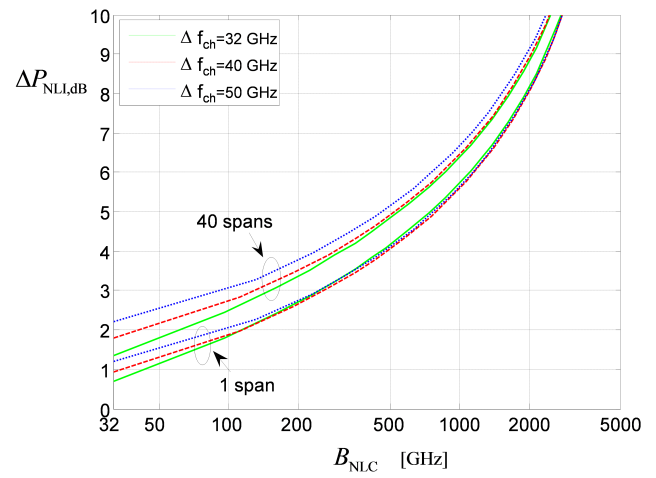


Fig. 14. Relative reduction of NLI, defined as $\Delta P_{\text{NLI,dB}}$ in Eq. (73), as a function of the non-linear optical compensation bandwidth B_{NLC} .

detailed MSR gain results are shown in Fig. 15, in terms of $\Delta N_{s,\text{dB}}^{\text{max}}$.

Overall, Fig. 15, appears to confirm the approximate prediction of Eq. (74). From a practical viewpoint, the obtained results indicate that achieving substantial performance gains is dauntingly difficult. Even assuming a Rx with a very large electrical bandwidth of 100 GHz, corresponding to $B_{\text{NLC}}=200$ GHz, the amount of MSR gain achievable in the analyzed scenarios reaches only 1.1 to 1.3 dB, depending on channel spacing. Conversely, if we set as goal that of achieving a doubling of the MSR (3 dB), then Fig. 15 shows that a minimum of 2 THz of optical compensation bandwidth should be taken into account by the NLC algorithm in order to obtain such gain. This would require combining the soft samples from multiple Rx’s but, even so, DSP complexity and power consumption would currently prove absolutely prohibitive.

To validate these analytical predictions, we ran a computer simulation of a specific scenario. We chose the case that, at the present state of technology, appears as the most realistically implementable. Specifically, we assumed single-Rx NLC, with B_{NLC} coinciding with a single-channel bandwidth. We simulated PM-16QAM with raised-cosine spectrum and roll-off 0.05. The channel spacing was $\Delta f_{\text{ch}}=33.6$ GHz. The Rx had an electrical matched filter prior to A/D conversion, to ensure that the value of B_{NLC} was exactly 32 GHz. DBP was applied, with 10 steps per span. In Fig. Fig. 16 we plot $\Delta N_{s,\text{dB}}^{\text{max}}$, vs. the number of channels in the system. The solid curve is analytical, whereas markers are simulations.

Theory and simulations agree very well, confirming the reliability of the GN-model in dealing with the NLC problem. On the specific topic of NLC performance, the model predictions, as well as the simulation results, are quite unfavorable, in the sense that gains are modest vs. the required optical bandwidth and resulting overall complexity. The GN-model provides a clear indication of why this is the case.

The outcome of our analytical investigation is in good general agreement with the simulative and experimental results reported in [73]-[77]. Note that actual implementations with limited complexity, like DBP with reduced number of steps

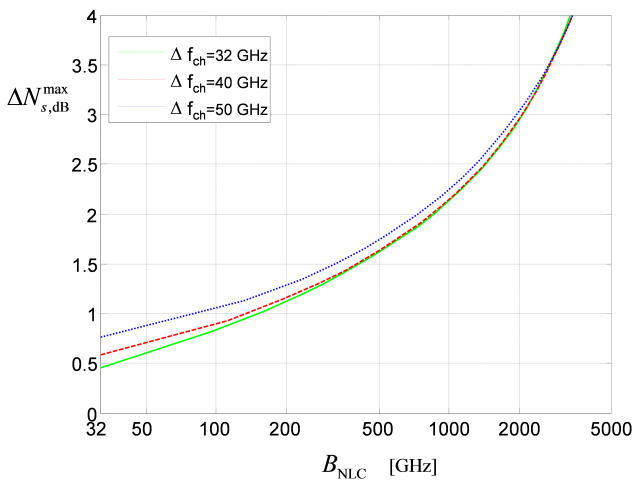


Fig. 15. Increase in maximum system reach (MSR) $\Delta N_{s,dB}^{\max}$, due to NLC, as a function of the NLC bandwidth B_{NLC} .

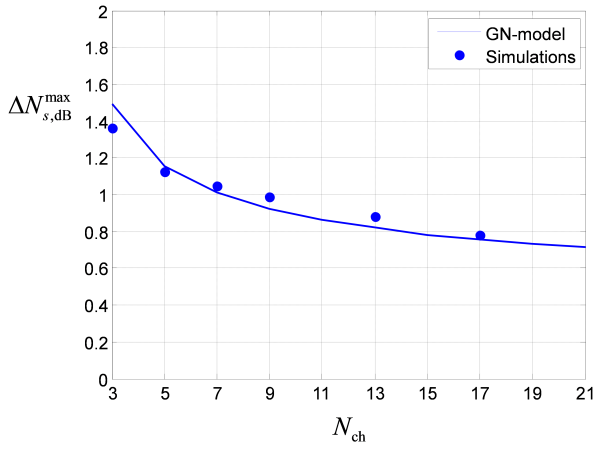


Fig. 16. Increase in maximum system reach (MSR) due to NLC, as a function of the number of channels N_{ch} in the system. The optical visibility band B_{NLC} coincides with a single channel. Solid curve: GN-model predictions. Markers: simulations results obtained using the DBP algorithm at 10 steps per span.

per span, in general show a reduced effectiveness, thus the results shown here have to be considered as an *upper bound* to the effectiveness of NLC. Moreover, our analysis neglected the effects of polarization-mode dispersion (PMD), which is not avoidable in practical fiber transmission and is known to reduce the effectiveness of non-linearity compensation algorithms [80], [81].

X. THE LOGON STRATEGY FOR FLEXIBLE NETWORKS

Although the GN-model is a strictly physical-layer oriented model, the implications of its availability may reach beyond the physical layer itself. In this section, we present an example of its potential impact on the overall network control and management.

In next-generation ‘flexible’ optical networks (NGFNs), based on coherent system, individual inter-node links will be populated with a variable number of channels with variable characteristics, such as format, symbol rate and perhaps chan-

nel spacing. In addition, routing of lightpaths will be optical and fast reconfigurability of such routing will be a must.

As a result, the problem of fast physical-layer reconfiguration and optimization becomes critical. For instance, the launch power per channel P_{ch} into each span should ideally be re-optimized according to the changing WDM comb characteristics. This function is typically attributed to a ‘physical-layer-aware’ Control Plane (CP) which, based on the future state of the overall network after a reconfiguration, should automatically optimize all values of P_{ch} . In fact, the CP should perform various other challenging tasks: it should assess the performance of each lightpath after any network reconfiguration, to find out whether sufficient signal integrity has been preserved. If not, the CP should carry out re-routing and possibly break up one or more lightpaths into multiple segments with regenerators in between.

In general, this would require the CP to have updated information on the entirety of the network, and take such information into account to perform global optimization. Interactions with higher layers may be necessary, to allocate traffic differently. Given the complexity of the CP assignments, and their criticality, it is clear that effective CP design is a key issue in NGFNs, and one on whose accomplishment the overall network performance hinges. Specifically, it is important to find ways to drastically reduce the complexity and computational effort of the CP, while preserving its effectiveness.

In this section we show that physical layer optimization and lightpath integrity assessment could be carried out in a simplified but still close-to-optimal way, with relatively small computational effort, thanks to GN-model derived results. We start out by discussing these issues for a single point-to-point link and then extend the found results to an overall network. We show that a Local Optimization strategy can lead close to a Global Optimum (LOGO strategy). We then introduce a simplified strategy that we call LOGON (where N stands for ‘Nyquist’), which is asymptotically optimum for high network spectral loads, with substantial potential for greatly simplifying and reducing the burden a CP must deal with. This section draws substantially from [82]. An experimental implementation of the concept was recently presented in [83].

A. The link optimization strategy

We assume incoherent NLI accumulation, that is, the IGN model. In a generic network, spans can be all different, so the link may not be homogenous. Also, in general, span loss may not be exactly in balance with span gain. As a result, the NLI PSD that we find at the Rx can be written as:

$$G_{NLI,Rx} = \sum_{n=1}^{N_{span}} G_{NLI,n} \Gamma_n \prod_{k=n+1}^{N_{span}} A_k \Gamma_k \quad (75)$$

where A_n is a number smaller than 1 accounting for the effect of loss in the n -th span, Γ_n is the (linear) gain of the EDFA following the n -th span and $G_{NLI,n}$ is the PSD of the NLI produced in the n -th span, *measured at the input of the n -th EDFA*, as shown in Fig. 17. Note the change of notation and meaning with respect to Eq. (9), where G_{NLI}^n was also the NLI PSD generated in the n -th span but *measured at the input of*

the Rx at the end of the link. Note also that the first EDFA is the one that follows the first span of fiber. In Eq. (75) the lower limit of the index k in the product symbol \prod overruns the upper limit when $n = N_s$. This causes no problem if, as customary, the product symbol \prod evaluates to 1 (and not to 0) when this happens.

ASE noise too is additive and hence it accumulates similarly to Eq. (75). As a result, the SNR at the Rx of anyone of the WDM channels in the link can be written as:

$$\text{SNR}_{\text{NL,Rx}} = \frac{P_{\text{ch,Rx}}}{R_s \sum_{n=1}^{N_s} \left[(G_{\text{ASE},n} + G_{\text{NLI},n} \Gamma_n) \prod_{k=n+1}^{N_s} A_k \Gamma_k \right]} \quad (76)$$

where $P_{\text{ch,Rx}}$ is the power of the channel under test (CUT) after the last EDFA (at the Rx input) and R_s is the symbol rate of that channel.

For convenience in performing the following steps, we concentrate on the quantity $\text{SNR}_{\text{NL,Rx}}^{-1}$. We also remark that $P_{\text{ch,Rx}}$ can be rewritten as follows, where m can be any value in $1 \dots N_s$:

$$P_{\text{ch,Rx}} = P_{\text{ch},m} \prod_{k=m}^{N_s} A_k \Gamma_k \quad (77)$$

where $P_{\text{ch},m}$ is the CUT power launched into the m -th span (see Fig. 17), being $P_{\text{ch},1}$ the CUT power launched into the first span by the Tx. Exploiting Eq. (77) to express $P_{\text{ch,Rx}}$ in Eq. (76), we can then write:

$$\text{SNR}_{\text{NL,Rx}}^{-1} = \frac{R_s \sum_{n=1}^{N_s} \left[(G_{\text{ASE},n} + G_{\text{NLI},n} \Gamma_n) \prod_{k=n+1}^{N_s} A_k \Gamma_k \right]}{P_{\text{ch},m} A_m \Gamma_m \prod_{k=m+1}^{N_s} A_k \Gamma_k} \quad (78)$$

Since the index m at the denominator is arbitrary, we can choose it to be equal to n and pull the denominator into the summation with the numerator:

$$\text{SNR}_{\text{NL,Rx}}^{-1} = \sum_{n=1}^{N_s} \frac{R_s (G_{\text{ASE},n} + G_{\text{NLI},n} \Gamma_n) \prod_{k=n+1}^{N_s} A_k \Gamma_k}{P_{\text{ch},n} A_n \Gamma_n \prod_{k=n+1}^{N_s} A_k \Gamma_k} \quad (79)$$

It can now be recognized that the products at the numerator and denominator cancel out. We also make the approximation: $G_{\text{ASE},n} \approx h\nu F_n \Gamma_n$, where F_n is the noise figure of the n -th EDFA, so that finally:

$$\text{SNR}_{\text{NL,Rx}}^{-1} = \sum_{n=1}^{N_s} \frac{R_s (h\nu F_n + G_{\text{NLI},n})}{P_{\text{ch},n} A_n} = \sum_{n=1}^{N_s} \frac{1}{\text{snr}_{\text{NL},n}} \quad (80)$$

where the quantity:

$$\text{snr}_{\text{NL},n} = \frac{P_{\text{ch},n} A_n}{R_s (h\nu F_n + G_{\text{NLI},n})} \quad (81)$$

is the SNR of the CUT at the output of the n -th EDFA, due to NLI produced exclusively in the n -th span and to the ASE noise of the n -th EDFA alone.

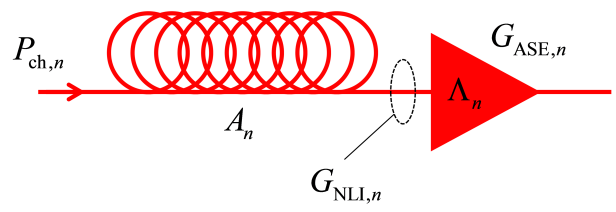


Fig. 17. Assumed span layout with the span-relevant quantities (see text).

Eq. (80) shows that the SNR at the Rx could be maximized by maximizing each one of the span SNRs individually. This optimization would greatly ease if the $\text{snr}_{\text{NL},n}$ were independent of one another. This is indeed the case, provided that we can assume that the WDM channel launch powers can be adjusted independently at each span. If so, we can arrange such powers so that each $\text{snr}_{\text{NL},n}$ is maximized. This is an important result, because it shows that local span optimization ensures global link SNR optimization, i.e., a LOGO strategy (local optimization - global optimization) can be used to perform whole link optimization.

Performing LOGO may however be somewhat problematic, because the specific dependence of $G_{\text{NLI},n}$ on the individual channel powers is, in general, rather complex. In the following we look for a simplified strategy which is based on pursuing $\text{snr}_{\text{NL},n}$ maximization under the assumption of full link spectral loading.

B. The LOGON strategy

We start out by considering the idealized case of full spectral loading. In NGFNs, full spectral loading is realized when the full available optical band B_{WDM} (typically the C-band or C+L) is utilized at maximum spectral efficiency. To model this situation, we assume that channel spectra are rectangular with bandwidth equal to the symbol rate R_s , and that frequency spacing is such that channel spectra touch but do not overlap, i.e., we assume the Nyquist limit. Channels may however still have different symbol rates or modulation formats.

In this special case, the GN-model predicts that $\text{snr}_{\text{NL},n}$ is optimized by launching a uniform signal PSD across the whole WDM comb. Such comb then spectrally appears as one seamless rectangle of overall bandwidth B_{WDM} and uniform PSD $G_{\text{WDM},n}$. The $\text{snr}_{\text{NL},n}$ for one specific WDM channel of symbol rate R_s , and the uniform optimum $G_{\text{WDM},n}$ which maximizes it, are:

$$\text{snr}_{\text{NL},n}^{\text{max}} = \frac{G_{\text{WDM},n}^{\text{opt}} A_n}{h\nu F_n + \mu_{\text{NLI},n} (G_{\text{WDM},n}^{\text{opt}})^3} \quad (82)$$

$$G_{\text{WDM},n}^{\text{opt}} = \sqrt[3]{\frac{h\nu F_n}{2\mu_{\text{NLI},n}}} \quad (83)$$

where μ_{NLI} , using the approximate Eq. (37), is written as:

$$\mu_{\text{NLI},n} = \frac{8}{27} \frac{A_n \gamma_n^2 L_{\text{eff},n}^2}{\pi |\beta_{2,n}| L_{\text{eff},a,n}} \text{asinh} \left(\frac{\pi^2}{2} |\beta_{2,n}| L_{\text{eff},a,n} B_{\text{WDM}}^2 \right) \quad (84)$$

The subscript n for all the physical parameters indicates that they are referred to the n -th span.

Eqs. (82)-(84), together with Eq. (80) essentially solve the problem of both optimizing the link and predicting its optimum performance, in closed form. They also show, once again, that such optimization can be done locally at each span. However, as pointed out, they apply to the case of full spectral loading. In general, the links of an optically-routed NGFN could be not fully loaded, or even lightly loaded, and a much more complex optimization would be needed.

A possible simplifying strategy, then, consists in using the above equations to perform link optimization in the network, irrespective of whether the links are actually fully loaded. We call such strategy LOGON, as it exploits LOGO under the assumption of Nyquist-limited full spectral loading.

Implementing LOGON requires ensuring that the launch power PSD at each span $G_{\text{WDM},n}^{\text{opt}}$ be that of Eq. (83). Note that under LOGON such value is completely static, because it is determined by fiber and EDFA built-in parameters while it is independent of the actual link spectral load. Enforcing $G_{\text{WDM},n}^{\text{opt}}$ could ideally be done by dedicated local hardware, without any CP intervention. The CP should in fact assume that Eq. (83) is indeed enforced and should carry out signal degradation estimation simply by using the rightmost side of Eq. (80). Each $\text{snr}_{\text{NL},n}$ in Eq. (80) is provided by Eq. (82) and such values are completely static and they are format, symbol rate and link spectral-load independent. They could be pre-computed and stored in memory as $\text{snr}_{\text{NL},n}$. To compute the $\text{SNR}_{\text{NL},\text{Rx}}^{-1}$ of any ‘lightpath’, possibly traveling through several nodes across the network, the CP would simply add up the $\text{snr}_{\text{NL},n}$ of all the spans traversed from Tx to Rx, an essentially instantaneous operation. The resulting $\text{SNR}_{\text{NL},\text{Rx}}$ could then be compared to the minimum required by the used transponder hardware to obtain spec-compliant channel BER. In this LOGON scenario, the CP becomes a thin and agile layer, whose main task is optimal routing under the constraint of large-enough $\text{SNR}_{\text{NL},\text{Rx}}$.

We point out that a substantial advantage of the LOGON strategy is that the insertion of one or more channels in an already partially populated link cannot cause any disruption nor can it require any re-routing of the channels already present in the link. This is because the NLI generated by the insertion of new channels is already factored in, to its worst (full-load) case, in the $\text{SNR}_{\text{NL},\text{Rx}}$ estimated for the already present channels. Their actual performance will of course degrade, but will be better or at worst equal to the $\text{SNR}_{\text{NL},\text{Rx}}$ that the CP has already considered.

This strength of LOGON is also its main weakness: by always assuming full spectral loading, when a lightpath travels across a sparsely populated network, its potential performance is substantially underestimated, possibly causing the CP to enact regeneration when it is not necessary. To assess such possible loss of performance, we examined five cases of link spectral under-filling, and computed how much performance underestimation was incurred, in terms of reach. In all cases, we assumed 100 km spans of typical SMF (see Table I) with EDFA noise figure 6 dB. Channels spectra were assumed rectangular with width equal to 32 GHz. In case I, a single

channel travels across a link that is completely unpopulated in all spans. Cases II and III consist of three and five adjacent channels, spectrally touching but not overlapping, and no other channels. Cases IV and V are links that are 33% and 50% populated in a uniform way across the whole C-band (assumed to be 5 THz), that is the channels are regularly separated by 64 or 32 GHz of empty spectrum, respectively. The results are shown in Table IV.

Apart from the extreme and rather unrealistic cases I and IV, performance underestimation is on the order of 20%. Ideally, if the CP monitored and adjusted each individual channel launch power in each span, this 20% of lost performance could be recovered. However, we point out that optimizing channels for ‘limit performance’ makes all the network routing quite fragile and load-dependent. A channel that reaches a certain transmission distance because the spans it goes through are scarcely populated, might no longer reach it when even just a single new channel is routed into just a single one of those spans. In ‘limit performance’ scenario, when lighting up a new channel, the CP would have to real-time re-calculate the performance of many already lit channels and take re-routing actions if any of them could no longer operate (the so called ‘crank-back’ procedure). This would in fact be a frequent occurrence if extreme optimization is performed in a highly loaded network. A single re-routing might in fact cause substantial disruption and generate the necessity of many further re-routings. The CP should operate globally even for local changes, the exact opposite of the LOGON strategy, with much higher resulting complexity.

The LOGON strategy has been recently used in an experimental testbed with good results in terms of predictivity and overall network optimization [83].

We point out that both LOGO and LOGON completely rely on results obtained in the GN-model context. They are clear examples of the practical impact that the availability of a simple but sufficiently accurate non-linearity model like the GN/IGN-model may have, all the way up to the network control level.

XI. COMMENTS AND CONCLUSIONS

In this paper we have pulled together the recent results regarding the GN-model definition, understanding and applications.

We showed that the GN-model is both the result of a collection of prior findings and of the re-consideration and extension of such findings.

We also focused on the key aspect of its validation. A detailed investigation of GN-model errors and limitations was proposed and extensively discussed. Overall, the GN-model accuracy for UT systems appears to be rather satisfactory and typically adequate for dealing with many practical scenarios.

The main source of error is the signal-Gaussianity approximation, used in the GN-model derivation, which is inaccurate especially in the initial part of a UT link. Research is ongoing on trying to find corrections that may account for the resulting discrepancies without requiring excessive added model complexity.

System Scenarios	Spectrum Filling	Empty Inter-Channel Band	MSR Prediction Error (in dB)	MSR Prediction Error (%)
I	single-channel	n/a	-1.75	-33%
II	3 adjacent channels	0	-1.12	-23%
III	5 adjacent channels	0	-0.92	-19%
IV	33%	64 GHz	-1.4	-27%
V	55%	32 GHz	-1	-20%

TABLE IV
MAXIMUM SYSTEM REACH PREDICTION ERROR USING LOGON

We collected and commented some of the GN-model closed-form approximate solutions, indicating their range of validity and limitations.

We finally devoted a quite substantial part of the paper to the description of several applications of the GN-model, all of which heavily exploit its closed-form approximate solutions. Specifically, we looked at link throughput analysis and optimization, at deriving approximate ‘design rules’ which provide a simple variational dependence of performance on system parameters, at finding the potential and limitations of non-linearity DSP-supported mitigation and, finally, at the use of the GN-model to derive an overall optimization and control strategy for new-generation optically-routed network. The breadth of these applications clearly demonstrates the extent of the impact of the availability of an effective model of non-linear propagation.

Research on modeling is ongoing and new models are constantly being proposed. Variations and improvements to the GN-model itself are also being proposed. In this context, we argue that the current GN-model offers a favorable accuracy vs. relative simplicity trade-off.

As a general remark, we observe that, already at their present stage, the results of the recent modeling efforts have quite radically changed the general understanding of the behavior of UT optical systems, as well as the way their analysis and design are approached.

XII. ACKNOWLEDGEMENTS

The authors would like to thank Jiang Yanchao for help in reformulating some of the results appearing in this paper. The authors would also like to thank Marco Schiano and Emilio Riccardi from Telecom Italia for the useful and insightful discussions.

APPENDIX A LIST OF ACRONYMS

AGN	additive Gaussian noise
AWGN	additive white Gaussian noise
ASE	amplified spontaneous-emission noise
BER	bit error-rate
BP	backward propagation
CP	network control-plane
CD	chromatic dispersion
DAC	digital to analog converter
DBP	digital back (or backward) propagation
DM	dispersion-managed
DSP	digital signal processing
EDFA	erbium-doped fiber amplifier

FEC	forward error-correcting code
FWM	four-wave mixing
GN-model	Gaussian-noise model
GNRF	GN-model reference formula
IDT	initial decoherence transient
IGN-model	incoherent Gaussian-noise model
IGNRF	GN-model reference formula
LOGO	local-optimization, global optimization
LOGON	LOGO with Nyquist-WDM
LWN	locally-white noise
ME	Manakov equation
MCI	multi-channel interference
MSR	maximum system reach
NGFN	new-generation flexible (optical) network
NLC	non-linearity compensation
NLI	non-linear interference
NLSE	non-linear Schroedinger equation
NZDSF	non-zero dispersion-shifted fiber
OCT	optical channel throughput
OFDM	orthogonal frequency-division multiplexing
OSNR	optical signal-to-noise ratio
PM	polarization-multiplexed
PSCF	pure-silica-core fiber
PSD	power spectral density
QAM	quadrature amplitude modulation
QPSK	quadrature phase-shift keying
Rx	receiver
SCI	self-channel interference
SE	spectral efficiency
SMF	standard single-mode fiber
SNR	signal-to-noise ratio
SPM	self phase modulation
SpS	spectral slicing
SR	system reach
TD	time-domain
Tx	transmitter
UT	uncompensated transmission
VS	Volterra series
WDM	wavelength-division multiplexing
XCI	cross-channel interference
XPM	cross phase modulation
XPolM	cross polarization modulation

REFERENCES

- [1] G. P. Agrawal, *Fiber-Optic Communications Systems*, 3rd ed. New York: Wiley, 2002.
- [2] D. Marcuse, C. R. Menyuk, P. K. A. Wai, ‘Application of the Manakov-PMD Equation to Studies of Signal Propagation in Optical Fibers with Randomly Varying Birefringence,’ *J. Lightwave Technol.*, vol. 15, no. 9, pp. 1735-1746, Sept. 1997.

- [3] J. P. Gordon and L. F. Mollenauer, 'Phase noise in photonic communications systems using linear amplifiers,' *Opt. Lett.*, vol. 15, no. 23, pp. 1351-1353, 1990.
- [4] D. Marcuse, 'Single-channel operation in very long nonlinear fibers with optical amplifiers at zero dispersion,' *J. Lightw. Technol.*, vol. 9, no. 3, pp. 356-361, Mar. 1991.
- [5] A. Mecozzi, 'Limits to longhaul coherent transmission set by the Kerr nonlinearity and noise of the inline amplifiers,' *J. Lightw. Technol.*, vol. 12, no. 11, pp. 1993-2000, Nov. 1994.
- [6] G. Bellotti, M. Varani, C. Francia, A. Bononi, 'Intensity Distortion Induced by Cross-Phase Modulation and Chromatic Dispersion in Optical-Fiber Transmissions with Dispersion Compensation,' *IEEE Photon. Technol. Lett.*, vol. 10, no. 12, pp. 1745-1747, Dec. 1998.
- [7] A. Cartaxo, 'Cross-phase modulation in intensity modulation-direct detection WDM systems with multiple optical amplifiers and dispersion compensators,' *J. Lightw. Technol.*, vol. 17, no. 2, pp. 178-190, Feb. 1999.
- [8] R. Hui, K. R. Demarest, and C. T. Allen, 'Cross-phase modulation in multispan WDM optical fiber systems,' *J. Lightw. Technol.*, vol. 17, no. 6, pp. 1018-1026, Jun. 1999.
- [9] P. P. Mitra and J. B. Stark, 'Nonlinear limits to the information capacity of optical fiber communications,' *Nature*, vol. 411, no. 6841, pp. 1027-1030, Jun. 2001.
- [10] E. E. Narimanov, P. P. Mitra, 'The channel capacity of a fiber optics communication system: Perturbation theory,' *J. Lightw. Technol.*, vol. 20, no. 3, pp. 530-537, Mar. 2002.
- [11] E. Desurvire, 'Quantum noise model for ultimate information-capacity limits in long-haul WDM transmission,' *Electron. Lett.*, vol. 38, no. 17, pp. 983-984, Aug. 2002.
- [12] A. Vannucci, P. Serena, and A. Bononi, 'The RP method: A new tool for the iterative solution of the nonlinear Schrodinger equation,' *J. Lightw. Technol.*, vol. 20, no. 7, pp. 1102-1112, Jul. 2002.
- [13] B. Xu and M. Brandt-Pearce, 'Comparison of FWM- and XPM-induced crosstalk using the Volterra series transfer function method,' *J. Lightw. Technol.*, vol. 21, no. 1, pp. 40-53, Jan. 2003.
- [14] K. S. Turitsyn, S. A. Derevyanko, I. V. Yurkevich, and S. K. Turitsyn, 'Information capacity of optical fiber channels with zero average dispersion,' *Phys. Rev. Lett.*, vol. 91, pp. 203901-1 to 203901-4, Nov. 2003.
- [15] A. Mecozzi, 'Probability density functions of the nonlinear phase noise,' *Opt. Lett.*, vol. 29, no. 7, pp. 673-675, 2004.
- [16] K.-P. Ho, 'Error probability of DPSK signals with cross-phase modulation induced nonlinear phase noise,' *IEEE J. Sel. Topics Quantum Electron.*, vol. 10, no. 2, pp. 421-427, Mar./Apr. 2004.
- [17] E. Forestieri and M. Secondini, 'Solving the nonlinear Schrödinger equation,' in *Optical Communication Theory and Techniques*, E. Forestieri, Ed. New York: Springer-Verlag, 2005, pp. 3-11.
- [18] E. Ciaramella and E. Forestieri, 'Analytical approximation of nonlinear distortions,' *IEEE Photon. Technol. Lett.*, vol. 17, no. 1, pp. 91-93, Jan. 2005.
- [19] S. Kumar, 'Effect of dispersion on nonlinear phase noise in optical transmission systems,' *Opt. Lett.*, vol. 30, no. 24, pp. 3278-3280, Dec. 2005.
- [20] K.-P. Ho and H.-C. Wang, 'Effect of dispersion on nonlinear phase noise,' *Opt. Lett.*, vol. 31, no. 14, pp. 2109-2111, July 2006.
- [21] A. T. Lau, S. Rabbani, and J. M. Kahn, 'On the statistics of intrachannel four-wave mixing in phase-modulated optical communication systems,' *J. Lightwave Technol.*, vol. 26, no. 14, pp. 2128-2135, July 2008.
- [22] M. Secondini, E. Forestieri, and C. R. Menyuk, 'A combined regular-logarithmic perturbation method for signal-noise interaction in amplified optical systems,' *J. Lightwave Technol.*, vol. 27, no. 16, pp. 3358-3369, Aug. 2009.
- [23] A. D. Ellis, J. Zhao, and D. Cotter, 'Approaching the non-linear Shannon limit,' *J. Lightwave Technol.*, vol. 28, no. 4, pp. 423-433, Feb. 2010.
- [24] A. P. T. Lau, T. S. R. Shen, W. Shieh, and K.-P. Ho, 'Equalization-enhanced phase noise for 100Gb/s transmission and beyond with coherent detection,' *Opt. Express*, vol. 18, no. 16, pp. 17239-17251, Aug. 2010.
- [25] L. Beygi, E. Agrell, M. Karlsson, and P. Johannisson, 'Signal statistics in fiber-optical channels with polarization multiplexing and self-phase modulation,' *J. Lightwave Technol.*, vol. 29, no. 16, pp. 2379-2386, Aug. 2011.
- [26] B. Goebel, R.-J. Essiambre, G. Kramer, P. J. Winzer, and N. Hanik, 'Calculation of mutual information for partially coherent Gaussian channels with applications to fiber optics,' *IEEE Trans. Inf. Theory*, vol. 57, no. 9, pp. 5720-5736, Sep. 2011.
- [27] G. Bosco, P. Poggiolini, A. Carena, V. Curri, and F. Forghieri, 'Analytical results on channel capacity in uncompensated optical links with coherent detection,' *Optics Express*, vol. 19, no. 26, pp. B438-B449, Dec. 2011.
- [28] A. Splett, C. Kurzke, and K. Petermann, 'Ultimate Transmission Capacity of Amplified Optical Fiber Communication Systems Taking into Account Fiber Nonlinearities,' in *Proc. ECOC 1993*, vol. 2, pp. 41-44, 1993.
- [29] H. Louchet et al., 'Analytical Model for the Performance Evaluation of DWDM Transmission Systems,' *IEEE Phot. Technol. Lett.*, vol. 15, no. 9, pp. 1219-1221, Sept. 2003.
- [30] M. Nazarathy, J. Khurgin, R. Weidenfeld, Y. Meiman, Pak Cho, R. Noe, I. Shpantzer, V. Karagodsky 'Phased-Array Cancellation of Nonlinear FWM in Coherent OFDM Dispersive Multi-Span Links,' *Optics Express*, vol. 16, pp. 15778-15810, 2008.
- [31] X. Chen and W. Shieh, 'Closed-Form Expressions for Nonlinear Transmission Performance of Densely Spaced Coherent Optical OFDM Systems,' *Optics Express*, vol. 18, pp. 19039-19054, 2010.
- [32] W. Shieh and X. Chen, 'Information Spectral Efficiency and Launch Power Density Limits Due to Fiber Nonlinearity for Coherent Optical OFDM Systems,' *IEEE Photon. Journal*, vol. 3, no. 2, pp. 158-173, Apr. 2011.
- [33] P. Poggiolini, A. Carena, V. Curri, G. Bosco, F. Forghieri, 'Analytical Modeling of Non-Linear Propagation in Uncompensated Optical Transmission Links,' *IEEE Photon. Technol. Lett.*, vol. 23, no. 11, pp. 742-744, June 2011.
- [34] A. Carena, V. Curri, G. Bosco, P. Poggiolini, F. Forghieri, 'Modeling of the Impact of Non-Linear Propagation Effects in Uncompensated Optical Coherent Transmission Links,' *J. of Lightw. Technol.*, vol. 30, no. 10, pp. 1524-1539, May. 2012.
- [35] P. Poggiolini, G. Bosco, A. Carena, V. Curri, Yanchao Jiang, F. Forghieri, 'A Detailed Analytical Derivation of the GN Model of Non-Linear Interference in Coherent Optical Transmission Systems,' posted on arXiv, www.arxiv.org, paper identifier 1209.0394. First posted Sept. 2012.
- [36] P. Poggiolini, 'The GN Model of Non-Linear Propagation in Uncompensated Coherent Optical Systems,' *J. of Lightw. Technol.*, vol. 30, no. 24, pp. 3857-3879, Dec. 2012.
- [37] A. Bononi, P. Serena, 'An Alternative Derivation of Johannisson's Regular Perturbation Model,' posted on arXiv, www.arxiv.org, paper identifier 1207.4729, July 2012.
- [38] P. Johannisson, M. Karlsson, 'Perturbation Analysis of Nonlinear Propagation in a Strongly Dispersive Optical Communication System,' *J. Lightwave Technol.*, vol. 31, no. 8, pp. 1273-1282, Apr. 15th 2013.
- [39] K.V. Peddaranappagari and M. Brandt-Pearce 'Volterra Series Transfer Function of Single-Mode Fibers,' *J. of Lightw. Technol.*, vol. 15, no. 12, pp. 2232-2241, Dec. 1997.
- [40] Jau Tang, 'The Channel Capacity of a Multispan DWDM System Employing Dispersive Nonlinear Optical Fibers and an Ideal Coherent Optical Receiver,' *J. Lightwave Technol.*, vol. 20, no. 7, pp. 1095-1101, July 2002.
- [41] Jau Tang, 'A Comparison Study of the Shannon Channel Capacity of Various Nonlinear Optical Fibers,' *J. Lightwave Technol.*, vol. 24, no. 5, pp. 2070-2075, May 2006.
- [42] A. Mecozzi, C. Balslev Clausen, M. Shttaif, 'Analysis of Intrachannel Nonlinear Effects in Highly Dispersed Optical Pulse Transmission,' *IEEE Phot. Technol. Lett.*, vol. 12, no. 4, Apr. pp. 392-394, 2000.
- [43] A. Mecozzi, C. Balslev Clausen, M. Shttaif, 'System Impact of Intrachannel Nonlinear Effects in Highly Dispersed Optical Pulse Transmission,' *IEEE Phot. Technol. Lett.*, vol. 12, no. 12, pp. 1633-1635, Dec. 2000.
- [44] A. Mecozzi, R.-J. Essiambre, 'Nonlinear Shannon Limit in Pseudolinear Coherent Systems,' *J. Lightwave Technol.*, vol. 30, no. 12, pp. 2011-2024, June 15th 2012.
- [45] A. Bononi, P. Serena, N. Rossi, E. Grellier, and F. Vacondio, 'Modeling Nonlinearity in Coherent Transmissions with Dominant Intrachannel-Four-Wave-Mixing,' *Optics Express*, vol. 20, pp. 7777-7791, 26 March 2012.
- [46] L. Beygi, E. Agrell, P. Johannisson, M. Karlsson, H. Wymeersch, 'A Discrete-Time Model for Uncompensated Single-Channel Fiber-Optical Links,' *IEEE Trans. on Commun.*, vol. 60, no. 11, pp. 3440-3450, Nov. 2012.
- [47] M. Secondini, E. Forestieri, "Analytical Fiber-Optic Channel Model in the Presence of Cross-Phase Modulations," *IEEE Photon. Technol. Lett.*, vol. 24, no. 22, pp. 2016-2019, Nov. 15th 2012.
- [48] P. Serena, A. Bononi, 'An Alternative Approach to the Gaussian Noise Model and its System Implications,' *J. Lightwave Technol.*, vol. 31, no. 22, pp. 3489-3499, Nov. 15th 2013.
- [49] A. Bononi and O. Beucher, 'Semi-analytic single-channel and cross-channel nonlinear interference spectra in highly-dispersed WDM coherent optical links with rectangular signal spectra,' posted on arXiv.org, paper arXiv:1309.0244, Sept. 2013.

- [50] R. Dar, M. Feder, A. Mecozzi, M. Shtaif, 'Properties of nonlinear noise in long, dispersion-uncompensated fiber links,' *Optics Express*, vol. 21, no. 22, pp. 25685-25699, Nov. 2013.
- [51] R. Dar, M. Feder, A. Mecozzi, M. Shtaif, 'Accumulation of nonlinear interference noise in multi-span fiber-optic systems,' posted on *arXiv.org*, paper arXiv:1310.6137, Oct. 2013.
- [52] G. Bosco, et al., 'Experimental Investigation of Nonlinear Interference Accumulation in Uncompensated Links,' *IEEE Photon. Technol. Lett.*, vol. 24, no. 14, pp. 1230-1232, Nov. 15th 2012.
- [53] K. Inoue, H. Toba, 'Fiber Four-Wave Mixing in Multi-Amplifier Systems with Nonuniform Chromatic Dispersion,' *J. Lightwave Technol.*, vol. 13, no. 1, pp. 88-93, Jan. 1995.
- [54] W. Zeiler, F. Di Pasquale, P. Bayvel, J.E. Midwinter, 'Modeling of Four-Wave Mixing and Gain Peaking in Amplified WDM Optical Communication Systems and Networks,' *J. Lightwave Technol.*, vol. 14, no. 9, pp. 1933-1942, Sept. 1996.
- [55] J. G. Proakis, *Digital Communication*. New York: McGraw-Hill, 1989.
- [56] S. Benedetto and E. Biglieri, *Principles of digital transmission: with wireless applications*, New York: Kluwer, 1999.
- [57] S. J. Savory, 'Approximations for the Nonlinear Self-Channel Interference of Channels With Rectangular Spectra,' *IEEE Phot. Technol. Lett.*, vol. 25, no. 10, pp. 961-964, May 15th 2013.
- [58] E. Torrenco, et al., 'Experimental Validation of an Analytical Model for Nonlinear Propagation in Uncompensated Optical Links,' *Optics Express*, vol. 19, no. 26, pp. B790-B798, Dec. 2011.
- [59] A. Nespola, et al., 'Extensive Fiber Comparison and GN-model Validation in Uncompensated Links using DAC-generated Nyquist-WDM PM-16QAM Channels', in *Proc. Opt. Commun. Conf.*, Los Angeles, paper OM3B.5, March 2013.
- [60] G. Bosco, A. Carena, V. Curri, R. Gaudino, P. Poggiolini, S. Benedetto, 'Suppression of Spurious Tones Induced by the Split-Step Method in Fiber Systems Simulation,' *IEEE Phot. Technol. Lett.*, vol. 12, no. 5, pp. 489-491, May 2000.
- [61] A. Carena et al., "Statistical Characterization of PM-QPSK Signals after Propagation in Uncompensated Fiber Links", in *Proc. of ECOC 2010*, paper P4.07, Torino (Italy), Sept. 2010.
- [62] F. Vacondio, C. Simonneau, L. Lorcy, J.C. Antona, A. Bononi and S. Bigo, 'Experimental characterization of Gaussian-distributed nonlinear distortions,' in *Proc. of ECOC 2011*, Geneva, paper We.7.B.1, Sept. 2011.
- [63] F. Vacondio, O. Rival, C. Simonneau, E. Grellier, A. Bononi, L. Lorcy, J.-C. Antona and S. Bigo, 'On nonlinear distortions of highly dispersive optical coherent systems,' *Optics Express*, Vol. 20, No. 2, pp. 1022-1032, Jan. 2012.
- [64] O. V. Sinkin, et al., 'Scaling of Nonlinear Impairments in Dispersion-Uncompensated Long-Haul Transmission,' in *Proc. of OFC 2012*, Los Angeles (US), paper OTu1A.2, Mar. 2012.
- [65] Olivier Rival, Kinda Mheidly 'Accumulation Rate of Inter and Intra-channel Nonlinear Distortions in Uncompensated 100G PDM-QPSK Systems,' in *Proc. Opt. Commun. Conf.*, OFC 2013, Los Angeles, paper JW2A.52, March 2013.
- [66] A. Carena, G. Bosco, V. Curri, P. Poggiolini, F. Forghieri, 'Impact of the Transmitted Signal Initial Dispersion Transient on the Accuracy of the GN-Model of Non-Linear Propagation,' in *Proc. of ECOC 2013*, paper Th.1.D.4, London (UK), Sept. 2013.
- [67] P. Serena, A. Bononi, 'On the Accuracy of the Gaussian Nonlinear Model for Dispersion-unmanaged Coherent Links' in *Proc. of ECOC 2013*, paper Th.1.D.3, London (UK), Sept. 2013.
- [68] C. E. Shannon, 'A mathematical theory of communication,' in *Bell Syst. Tech. J.*, vol. 27, pp. 379-423 1948.
- [69] R.-J. Essiambre, G. Kramer, P. J. Winzer, G. J. Foschini, B. Goebel, 'Capacity limits of optical fiber networks,' *J. Lightwave Technol.* vol. 28, pp. 662-701, 2010.
- [70] Erik Agrell, 'Nonlinear Fiber Capacity,' in *Proc. of ECOC 2013*, London (UK), paper We.4.D.3, Sept. 2013.
- [71] X. Zhou et al., 'High Spectral Efficiency 400 Gb/s Transmission Using PDM Time-Domain Hybrid 32-64 QAM and Training-Assisted Carrier Recovery,' *J. Lightw. Technol.*, vol. 31, no. 7, Apr.1 2013, pp. 999-1005.
- [72] S. Savory, 'Digital filters for coherent optical receivers,' *Opt. Express*, vol. 16, no. 2, pp. 804-817, 2008.
- [73] E. Ip, J.M. Kahn, 'Compensation of Dispersion and Nonlinear Impairments Using Digital Backpropagation,' *J. Lightw. Technol.*, vol. 26, no. 20, Oct. 2008, pp. 3416-3425.
- [74] S. J. Savory et al., 'Impact of Interchannel Nonlinearities on a Split-Step Intrachannel Nonlinear Equalizer,' *J. Lightw. Technol.*, vol. 22, no. 10, May.15 2010, pp. 673-675.
- [75] D. Rafique, J. Zhao, D. Ellis, 'Digital back-propagation for spectrally efficient WDM 112 Gbit/s PM m-ary QAM transmission,' *Opt. Express*, vol. 19, no. 6, pp. 5219-5224, 2011.
- [76] H. Zhang, et al., '200 Gb/s and Dual-Wavelength 400 Gb/s Transmission over Transpacific Distance at 6 b/s/Hz Spectral Efficiency,' in *Proc. of OFC 2013*, Anaheim, paper PDP5A.6, Mar. 2013.
- [77] J.-X. Cai, et al., 'Nonlinearity Compensation Benefit in High Capacity Ultra-Long Haul Transmission Systems,' in *Proc. of ECOC 2013*, paper We.4.D.2, London (UK), Sept. 2013.
- [78] J. Reis, A. Teixeira, 'Unveiling nonlinear effects in dense coherent optical WDM systems with Volterra series,' *Optics Express*, vol. 18, no. 8, pp. 8660-8670, Apr. 2010.
- [79] N. Stojanovic et al., 'MLSE-based nonlinearity mitigation for WDM 112 Gbit/s PDM-QPSK transmission with digital coherent receiver,' in *Proc. Opt. Commun. Conf.*, Los Angeles, paper OWW6, March 2011.
- [80] G. Gao, X. Chen, W. Shieh, 'Influence of PMD on nonlinearity compensation using digital back propagation,' *Optics Express*, vol.20, pp.14406-14418, 2012.
- [81] Fatih Yaman, Guifang Li, 'Nonlinear Impairment Compensation for Polarization-Division Multiplexed WDM Transmission Using Digital Backward Propagation,' *IEEE Photonics J.*, vol. 2, no. 5, pp. 816-832, Oct. 2010.
- [82] P. Poggiolini, G. Bosco, A. Carena, R. Cigliutti, V. Curri, F. Forghieri, R. Pastorelli, S. Piciaccia, 'The LOGON Strategy for Low-Complexity Control Plane Implementation in New-Generation Flexible Networks,' in *Proc. of OFC 2013*, paper OW1H.3, Los Angeles (CA), March 2013.
- [83] R. Pastorelli, et al., "Optical Control Plane Based on an Analytical Model of Non-Linear Transmission Effects in a Self-Optimized Network," in *Proc. of ECOC 2013*, paper We.3.E.4, London (UK), Sept. 2013.